Applied Water Science (2024) 14:80
https://doi.org/10.1007/s13201-024-02140-3

ORIGINAL ARTICLE

Efficient removal of *E. coli* from wastewater by novel phytofabricated nano-zinc using antibacterial potential, kinetic studies, and response surface methodology

Safaa M. Ezzat[1] · **Mohammed T. Moustafa**[1]

Received: 3 December 2023 / Accepted: 16 February 2024 / Published online: 19 March 2024

Abstract
The present investigation explores the antibacterial potential of novel ZnO-NPs synthesized from *Acacia nilotica* pods extract and immobilized onto sodium alginate beads to control bacterial pollution in wastewater. Phenolics and flavonoids were major phytoconstituents acting as capping, reducing, and stabilizing agents. UV–Vis analysis showed strong absorption band at 340 nm. XRD and TEM revealed hexagonal crystalline structure for zincite of average particles diameter 33.87 and 32.74 nm, respectively. FTIR demonstrated several bands with functional groups (O–H, C-H, C = O, C = C, and C–O–C) involved in ZnO-NPs synthesis. SEM images showed NPs surface completely colonized by *E.coli*, while EDX spectrum showed signals for zinc (52.94%) and oxygen (26.58%) confirming NPs purity. Adhesion capacity studies revealed ZnO-NPs potential (0.5 g) to remove *E.coli* after 120 min. Kinetic and isotherm studies indicated that pseudo-second-order model and Freundlich isotherm were best fit describing adhesion mechanism. Electrostatic attraction between negatively charged *E.coli* and positively charged ZnO-NPs was followed by generation of H_2O_2 leading to cell apoptosis. Adhesion optimization using Box–Behnken design under response surface methodology was 99.8% at disinfectant dose 30 g/L, contact time 6 h, and *E.coli* concentration 150×10^7 cfu/mL. For application, real wastewater was treated with removal 98.2%, 97.2%, and 96.5% for total coliform, fecal coliform, and *E.coli*, respectively, after 6 h. ZnO-NPs showed sustainable efficiency during four consecutive cycles of treatment. The study concluded the efficiency, eco-friendly and cost-effectiveness of phytofabricated ZnO-NPs as disinfectants for wastewater and recommended future studies on large scale for possible wastewater reuse in safe unrestricted irrigation.

Keywords *Acacia nilotica* · Adhesion · *Escherichia coli* · Kinetics · Wastewater disinfection · Zinc oxide nanoparticles

Introduction

Microbial contamination of water resources is regarded as serious concern on human health particularly when water is intended for use in drinking or irrigation purposes. In addition, water scarcity and shortage exert non-ignorable pressure on this vital sector that necessitates focused efforts in water management and treatment strategies (Nikel and Eltahir, 2021). Water resources exposed to wastes discharge are likely prone to the bacteria *Escherichia coli* (*E. coli*), whose concentration may reach 2×10^6 CFU/100 mL of water. Being important water-borne pathogen, it is potentially the causative agent of high cases of gastroenteritis and urinary tract diseases. Moreover, it is reported in long-term hospitalized patients as well as those detained in intensive care units. Accordingly, wastewater discharged from hospitals is mostly suspected of harboring antibiotics resistant *E. coli* strains (Ma et al.2022).

Currently, several treatment technologies are applied to eliminate pathogenic bacteria from water. The most important are chlorination, ozonation, ultraviolet-based disinfection, and membrane separation. Although chlorination is considered a universally used disinfectant, however it can generate potential carcinogenic by-products in the presence of organic matter contaminates. On the other hand, ozone

✉ Safaa M. Ezzat
dr-safaa-ezzat@hotmail.com

Mohammed T. Moustafa
mohammedtaha2010@outlook.com

[1] Microbiology Department, Central Laboratory for Environmental Quality Monitoring (CLEQM), National Water Research Center (NWRC), P.O. Box 13621, El-Qanater, Egypt

water treatment is extremely energy-intensive, highly reactive, and cost-prohibitive in operation and maintenance. Concerning UV-based disinfection, it is not considered the right choice in case of cloudy water. Meanwhile, the prolonged use of membrane separation may lead to biofouling and interference with disinfection efficiency as well as economic feasibility (Wang et al. 2018).

Due to the drawbacks of the aforementioned treatment methods, nanotechnology nowadays presents a new horizon in the field of water disinfection. This growing field has attracted researches to focus on the synthesis, design, and particles structure manipulation ranging from 1 to 100 nm, and to apply in water treatment and purification protocols. Nanoparticles (NPs) have piqued interest as remarkable antibacterial agents even at very low concentrations, owing to their high surface to volume ratio as well as their unique physicochemical properties (Wang et al. 2017). Some of these NPs are recognized as non-toxic, and even more contain trace elements essential for vital activities in the human body. Metallic nanoparticles bearing such characteristic features are Zinc oxide nanoparticles (ZnO-NPs).

ZnO-NPs have been reported as active agents against a wide range of microorganisms including: *Escherichia. coli, Pseudomonas aeruginosa, Bacillus subtilis, Staphylococcus aureus, Bacillus megaterium, Klebsiella pneumonia, Pseudomonas vulgaris, Candida albicans, Sarcina lutea, and Aspergillus niger* (Siddiqi et al. 2018). The nanocomposite chitosan-zinc oxide with 10% ZnO proved to be an efficient and eco-friendly biocide capable of inhibiting biofilms growth of sulfate reducing bacteria and mitigating excessive bio-corrosion on carbon steel surfaces (Rasheed et al. 2019). The mechanism of action of ZnO-NPs appears to be through increasing the reactive oxygen species produced by bacteria, which in turn elevate membrane lipid peroxidation, thus stimulating membrane leakage of reducing sugars, proteins, DNA, and interfere with cell viability (Rasha et al. 2021).

ZnO-NPs have displayed better biocompatibility compared to other nanoparticles. For example, ZnO-NPs showed a higher photocatalytic performance than TiO_2-NPs regarding photodegradation of pollutants due to their high electron mobility and low valence bond position (Mallakpour et al. 2021). Owing to their distinguished environmentally friendly and physicochemical properties, ZnO-NPs have been widely employed in several commercial and additive products. These products include ceramics, glass, sealants, cement, pigments, plastics, adhesives, batteries, electronic transistors, catalysis, lubricants, biosensors, cosmetics, ointments, and sunscreens (Zhou et al. 2023). Recently, studies on the potential of ZnO-NPs as additives in grain crops concentrate mainly on antimicrobial activity, nutritional enhancement, and stress resistance (Salam et al. 2022(. ZnO nano-composites could effectively inhibit the proliferation and growth of dominant microorganisms in maize storage particularly fungi such as *Aspergillus flavus*, *Talaromyces variabilis*, *Penicillium citrinum*, *and Fusarium graminearum* (Zhang et al. 2024).

It is worth noticing that the safety of ZnO-NPs was reported by the US Food and Drug Administration (FDA-21CFR182.8991), with no evidences of carcinogenicity, reproduction toxicity/and or genotoxicity in humans (Araujo-Lima et al. 2017; Lopes de Romana et al. 2002). The FDA categorized ZnO-NPs as GRAS (generally recognized as safe) and declared them as biocompatible antimicrobials due to their minimal toxicity (Akbar et al. 2021). Hence, they are used in medicine, food packaging, and cosmetics (Espitia et al. 2015; Singh et al. 2020). In the European Union, a study was conducted by EFSA (European Food Safety Authority) to investigate the safety of ZnO-NPs for several applications in food contact materials. The study concluded that zinc does not migrate in nano-form, and hence, the safety evaluation should focus on migration of soluble ionic zinc. The study recommended to impose an upper limit of zinc (25 mg/person/ per day) as safe daily dose (Souza et al. 2020).

Metals oxide NPs as ZnO have been traditionally prepared using several physicochemical methods as, for example, simple precipitation, co-precipitation, mechanical milling, electrochemical synthesis, sol–gel, hydrothermal methods, and others (Hessien et al. 2022). Physical and chemical methods are often complicated and expensive. In addition, some of them use high radiation and high concentrations of reducing and stabilizing agents and may release toxic by-products during synthesis that threaten human health and harm the environment. In comparison, "biosynthesis" or "green synthesis" of NPs using plants extracts has been proven promising alternative to conventional methods. It is eco-friendly, cost-competitive, energy saving, and can be formed at ambient temperature and neutral pH conditions. Furthermore, the reaction rate is relatively fast and can be smoothly scaled up for high production of NPs (Ettadili et al. 2022). Bioactive phytochemicals present in plants extracts are believed to play a principle role in reducing and capping the used metallic ions as well as stabilizing them. These phytochemicals include polyphenols, phenolic acids, carboxylic acids, alkaloids, saponins, terpenoids, polysaccharides, proteins, and lipids (Hemlata et al. 2020).

The superiority of green synthesis over microbial synthesis of ZnO-NPs has been studied using aqueous leaf extract of *Cochlospermum religiosum*. The plant extract and the biofabricated ZnO-NPs showed significant inhibition potential against several Gram-positive (*Staph. aureus* and *B. subtilis*) as well as Gram-negative (*E. coli* and *P. aeruginosa*) bacteria (Mahendra et al. 2017).

Acacia nilotica (L.) Delile, commonly known as "babul" or "Kiker," is widely distributed in tropical and subtropical regions in Africa, Asia, and Australia. It

belongs to the family *Fabaceae* and considered native of Egypt (Egyptian mimosa or Egyptian thorn). It grows along the banks of Nile River, Red Sea coastal zone, as well as Sinai, and many parts of the Egyptian deserts (Batanouny 1999). Due to its nature as a versatile source for several bioactive compounds, it has been reported as an important medicinal plant and was used traditionally to treat leucodermal diseases, bleeding piles, diarrhea, dysentery, cough, sore throat, hemorrhage, and diabetes.

Acacia nilotica is one of the plants whose extracts are known to be rich in antimicrobial compounds and has been reported to be potent against bacteria, fungi, viruses, and parasites in several studies (kaur et al. 2022). In a study, the use of 10% of the methanolic extract of *Acacia nilotica* pods showed a superior bactericidal effect (around 100%) against some important antibiotic resistant bacteria including *Klebsiella* spp, *E. coli*, and methicillin-resistant *Staphylococcus aureus*. Another in vitro study investigated the antibacterial activity of the hot ethanolic extract on the growth of several bacterial species of medical importance using the agar well-diffusion assay. Using 100 mg/ml of the extract was capable of inhibiting the growth of *Streptococcus pneumonia*, *Proteus mirabilis*, and *Staphylococcus aureus*. In comparison, 75 mg/ml was efficient to inhibit both *E. coli* and *Pseudomonas aeruginosa* (Abduljawad 2020).

Though *Acacia nilotica* extracts have earlier been evaluated for their antibacterial activities, only limited studies have investigated their potential as bioreductants to mediate NPs synthesis. Different parts of the plant were used in this purpose and included the pods, the leaves, the bark, and the aerial parts to prepare silver, gold, iron, and copper oxide NPs, as well as silver-doped titanium oxide and zinc oxide–copper oxide nanocomposites. Nearly most of the applications were dedicated to medicinal activities (Arya et al. 2019; Abduljawad 2020). To the best of our knowledge, no attempts have been carried out to evaluate the potency of these nanomaterials as disinfectants for wastewater.

Hence, the present work aims to report the green synthesis of ZnO-NPs immobilized by sodium alginate from the aqueous extract of *Acacia nilotica* pods and to elucidate the antibacterial potential of these biogenic nanomaterials as novel disinfectants for wastewater and elimination of *E. coli*. The optical and morphological characterizations of phytofabricated NPs are studied. The kinetics dynamics and adhesion isotherms of *E. coli* from wastewater onto ZnO-NPs are investigated to elaborate the removal mechanism. Finally, the response surface methodology is used as a following step to optimize the disinfection efficiency. We expect the phytofabricated nanomaterial we present to offer a smart and cost-effective management for microbial wastewater pollution in accordance to the aims of reusability and sustainability in safe unrestricted irrigation.

Materials and methods

Preparation of plant extract

Samples of *Acacia nilotica* pods proposed for phytofabrication of ZnO-NPs were collected from a specialized official botanical garden of Faculty of Pharmacy, Cairo University, Egypt. The selected pods were washed thoroughly using running tap water 2–3 times, and then with distilled water and subjected to drying in oven (40 °C) till constant weight (Al-Samarrie et al. 2012). Using an electric mixer, the dried pods were pulverized and kept away from moisture in dry closed glass containers till use.

To prepare the required phytoextract, water was chosen as extraction solvent, being green and eco-friendly, cost-effective, and easily available. About 10 g of dried pulverized pods were mixed with 100 mL of sterile boiled distilled water in 500-mL Erlenmeyer flasks. The flasks were shaken well by vortex for 15 min and allowed to stand for 6 h at ambient room temperature. The extract obtained was then filtered through muslin cloth (double-layered) twice, followed by filter paper Whatman No. 1, and sterilized using cellulose nitrate filter (Sartorius) 0.45 µm (Ahmad and Beg 2001).

Phytochemical analysis of plant extract

The preliminary phytochemical analysis was carried out as per earlier procedures reported by Harborne (1998). The aqueous extract of *Acacia nilotica* pods was examined to identify the active constituents that might contribute to its antibacterial activity and its potential for acting as capping and reducing agents in NPs synthesis. The tested compounds were recorded as present or absent and included tannins, steroids, terpenoids, flavonoids, phenols, alkaloids, glycosides, carbohydrates, saponins, anthraquinones, and resins. Further investigations concerning the phenolic constituents were conducted using the high-performance liquid chromatography (Hewlett Packard HPLC-1100) analysis. Phenolic compounds were identified by comparing their relative retention times with those of the standard mixture chromatograms. The concentration of an individual compound was calculated on the basis of peak area measurement, and then converted to µg/100 g dry weight. All chemicals and solvents used were HPLC spectral grade. Standard phenolic compounds were obtained from Sigma-Aldrich (St. Louis, USA) and from Merck Schuchardt (Munich, Germany) chemical companies.

Synthesis of phytofabricated zinc oxide nanoparticles (ZnO-NPs)

Zinc nitrate hexahydrate ($Zn(NO_3)_2 \cdot 6H_2O$) was used to synthesize ZnO-NPs. 11.8 g of 1 M of $Zn(NO_3)_2 \cdot 6H_2O$ was

dissolved in 40 mL of water and mixed well with a magnetic stirrer. To this mixture, 10 mL of *Acacia nilotica* pods extract were added drop by drop using a sterile injector. The resulting mixture was stirred for 20 min in continuous manner. Sodium hydroxide (NaOH) solution (2 M) was added dropwise to the above solution. After the completion of the reaction, the mixture was allowed to precipitate for 24 h. The precipitate was separated by centrifugation at 4000 rpm for 15 min and washed repeatedly with distilled water and dried at 80 °C in a hot air oven. The obtained powder was grinded with a mortar into fine powder and calcinated in muffle furnace at 350 °C for 3 h to obtain fine ZnO-NPs (Pachaiappan et al. 2021).

Antibacterial activity studies

The extract of *Acacia nilotica* pods and the phytofabricated ZnO-NPs was tested for their antibacterial activity using gram-negative bacteria (*E. coli* ATCC 25922) by the agar well-diffusion method. The bacterial test organism was grown in nutrient broth for 24 h; after that the bacterial suspension (10 CFU/ mL) was swabbed over the surface of agar plates. Agar wells of 8-mm diameter were prepared with the help of a sterile cork borer (Perez et al 1990). The dry plant extract and the ZnO-NPs fine powder were re-constituted in distilled water (sterile) to give the following concentrations (100, 200, 300, and 400 mg/ mL), and then 100 µL of each corresponding concentration were injected in agar wells. For comparative study, 100 µL of sterile distilled water was used as a negative control, along with 100 µL of 30 µg/mL of the antibiotic streptomycin as a positive control. Three replicate plates were tested for each treatment, and the Petri dishes were immediately incubated at 35 °C for 24 h and then examined for the presence of inhibition zones. The zone of clearance diameter for each test was recorded and measured in millimeter (mm) using a graduated ruler.

Characterization of phytofabricated ZnO-NPs

To validate the formation of phytoassisted ZnO-NPs, the following techniques were applied: (1) measuring the UV–Vis spectrum using UV Orion Aquamat 8000 spectrophotometer—Thermo Fisher Scientific (USA)—operated at range from 190 to 1100 nm; (2) the X-ray diffraction (XRD) analysis was performed on X-ray diffractometer—PANalytical X'Pert Pro (UK); (3) the presence of major active functional groups in *Acacia nilotica* extract-mediated ZnO-NPs formation was revealed by Fourier transform infrared (FTIR) analysis performed on spectrometer (Bruker-VERTEX 80 V) in range of 900 cm^{-1} to 5 cm^{-1}; (4) the surface morphology of nanoparticles was examined by scanning electron microscope (SEM) Quanta 250 FEI Company, coupled with energy-dispersive X-ray (EDX) spectroscopy to diagnosis the crystals purity, size, and structure; (5) the corporal properties of the synthesized ZnO-NPs were analyzed by the transmission electron microscope (TEM) JEOL JEM-2100.

Immobilization of phytofabricated ZnO-NPs onto sodium alginate

Sodium alginate (SA) beads were prepared by dissolving 3 g of SA in 100 mL of distilled water under continuous magnetic stirring for 1 h. The mixture was then sterilized by autoclaving, and ZnO-NPs (10 mL) were added and further stirred for 30 min. The gel beads (ZnO/SA) were generated by dropping the mixture into 100 mL $CaCl_2$ solution with stirring at 100 rpm, followed by incubation for 24 h at 4 °C (Natrah et al. 2020).

Adhesion capacity

E. coli (ATCC 25923) was chosen to study the adhesion capacity onto ZnO-NPs at different time intervals. *E. coli* (ATCC 25923) was provided by the microbiology department of Central Laboratory for Environmental Quality Monitoring (CLEQM), National Water Research Center (NWRC). The *E. coli* cells were cultured in Erlenmeyer conical flasks containing 100 mL of nutrient broth at 37 °C over 24 h. The obtained growth was diluted to a concentration of 254×10^7 CFU/mL. 0.5 g of ZnO-NPs were added to 10 mL of the *E. coli* suspension and shaken by hand to assure proper mixing. The suspension was then allowed to stand for 15, 30, 60, 90 and 120 min. 100 µL samples were separately plated onto agar and incubated at 37 °C for 24 h. The resulting plate counts were used to estimate the concentrations of *E. coli* in the tube at each time point. All experiments were performed in triplicates. The number of *E. coli* cells adhering was estimated using the difference between the number of colonies in the suspension before and after the adhesion experiments. The adhesion capacity of ZnO-NPs for *E. coli* is calculated according to (Wang et al. 2018) using Eq. (1):

$$q_{t=}\left[C_i - C_t\right]/m \tag{1}$$

q_t represents the adhesion capacity for *E. coli* cells after interval t, C_i and C_t are the initial number of *E. coli* cells and the residual number at time (t), and m represents the mass of ZnO-NPs.

Adhesion kinetics

For the analysis of experimental kinetics data, two kinetic models were applied: the pseudo-first-order kinetics which describes the initial stage of the adhesion process, and the pseudo-second-order kinetics which gives appropriate

description of the whole adhesion process based on data generated from the adhesion capacity studies (Wang et al. 2018).

Adhesion isotherms

In the present study, the adhesion equilibrium data were fitted using the Langmuir and Freundlich models to investigate the adhesion of *E.coli* from wastewater onto ZnO-NPs. The Langmuir model is an empirical model based on the assumption that adhesion takes place on the surface of the adsorbent where uniform energy sites are available. Meanwhile, the Freundlich model assumes that multilayer adhesion occurs due to diversity of adhesion sites (Archana et al. 2022).

Response surface methodology (RSM)

In order to study the effect of operating parameters controlling the adhesion of *E. coli* from wastewater onto ZnO-NPs and subsequently maximize the system removal efficiency, the response surface methodology (RSM) was applied using the Box–Behnken design (BBD) to identify the relation between independent variables and the measured response. RSM is integration between mathematical and statistical tools in order to determine the optimum conditions needed for conducting the required experiment with the least number of runs and to achieve maximum potential for the desired response (Jafari et al. 2016).

In this investigation, three variables were used as the design of the model experiments;

(A: disinfectant dose; B: *E. coli* concentration; and C: contact time). Each variable was set with three levels: low (− 1), middle (0), and high (+ 1). Disinfectant dose (10–30 g/L), initial *E. coli* concentration (75–300 × 10^7 cfu/mL), and contact time (1–6 h) were considered as input variables. The experimental design derived from BBD showing the ranges and the levels of independent variables are presented in Table 1. A total of 17 experiments were conducted, and the removal percentage of *E. coli* from wastewater was considered as the system response.

The behavior of the removal process can be elucidated through the second-order polynomial equation as follows:

$$Y = b_0 + \sum_{i=1}^{n} b_i x_i + \sum_{i=1}^{n} b_{ii} x_i^2 + \sum_{i=1}^{n-1} \sum_{j=i+1}^{n} b_{ij} x_i x_j \quad (2)$$

Y: the predicted response (*E. coli* removal efficiency); b_0: the constant coefficient; b_i: regression coefficient for linear effect; b_{ii}: quadratic coefficient; b_{ij}: interaction coefficient; and x_i, and x_j: the coded values of variables.

The analysis of variance (ANOVA) was performed at 95% confidence level to evaluate the sufficiency and significance of the regression model. The determination coefficient (R^2) was calculated to evaluate the model's fitness, and the *F*- and *P*-values were used to confirm statistical significance. Finally, the 3D plots of response versus independent variables were generated to predict the best operating design.

Wastewater disinfection and reusability studies

Wastewater samples were collected from El- Rahawy drain, Giza governorate, Egypt. Sampling procedure and water analyses were carried out following the instructions of Standard Methods for the Examination of Water and Wastewater (APHA 2017). The collected samples were preserved in an iced cooler box and delivered immediately to the Central Laboratory for Environmental Quality Monitoring (CLEQM), National Water Research Center (NWRC) to be analyzed within 6 h. Bacteriological parameters considered for evaluating the microbiological quality of wastewater samples included total coliforms (TC), fecal coliforms (FC), and *E. coli*. The membrane filtration assay was applied in accordance with standard methods No. 9222B, 9222D, and 9213 D, respectively. The appropriate volumes of tested samples were filtered through 47-mm cellulose nitrate membrane filter (Sartorius), with 0.45-µm pore size. The plates of TC were incubated on m-Endo Agar LES (at 35 °C for 24 h), FC on M FC Agar (at 44.5 °C for 24 h), while the *E. coli* on modified m-TEC Agar (at 44.5 °C for 24 h). All processed media were available from Merck, Germany, and Difco™. The obtained results were reported as colony-forming unit (CFU/100 mL) using Eq. (3):

$$\text{Colonies/100 ml} = \frac{\text{counted colonies}}{\text{ml of sample filtered}} \times 100 \quad (3)$$

Table 1 Matrix of the Box–Behnken design for *E. coli* removal

Variables	Codes	Range and levels		
		Low level (− 1)	Central level (0)	High level (+ 1)
Disinfectant dose (g/L)	*A*	10	20	30
Initial *E. coli* concentration (cfu/mL)	*B*	75 × 10^7	150 × 10^7	300 × 10^7
Contact time (hours)	*C*	1	3	6

The potential of phytofabricated ZnO-NPs immobilized onto SA for disinfection of wastewater samples was tested by adding about 30 g of ZnO/SA gel beads to one liter of wastewater in a glass reactor for different contact time intervals (1, 3, 6, and 24 h). To accomplish this step, the reactor was subjected to a magnetic stirrer at 190 rpm, and all experiments were done in triplicates. The microbiological quality of treated wastewater was evaluated, and the removal efficiency of bacterial indicators (TC, FC, and *E. coli*) was expressed as percentage removal (R %) and calculated using Eq. (4):

$$R(\%) = C_i - C_f / C_i \times 100 \quad (4)$$

where C_i and C_f are the initial and final count of bacteria, respectively.

In order to determine the reusability range of phytofabricated immobilized ZnO-NPs, *E. coli* was chosen as an important indicator for these experiments. About 30 g of nano-ZnO/SA gel beads were soaked in one liter of wastewater under mechanical stirring at 190 rpm for 6, 8, 12, and 24 h. The gel beads of immobilized NPs used were easily washed with deionized water and reused in new disinfection runs, where four consecutive cycles were accomplished. Each time, the count of *E. coli* was reported, and the removal efficiency was calculated as previously described in Eqs. (3) and (4), respectively.

Statistical analysis

All experiments were repeated in triplicates. Data were expressed as mean values ± standard errors using the Statistical Package for the Social Sciences (SPSS) version 18.0 including one-way ANOVA test for the normally distributed data at 0.05 level to determine the significance between different means.

Results and discussion

Phytochemical analysis of *Acacia nilotica* extract

Keeping in view the objective of this investigation, the selected (*Acacia nilotica* pods) was subjected to chemical analysis to identify the possible reducing phytochemicals presumably involved in NPs synthesis. The dry weight of the plant extract was 2.27 g, and the percentage of extracted material was 22.7%. Data from preliminary phytochemical screening demonstrated in Table 2 revealed the presence of ten broad chemical groups. The identified groups included alkaloids, flavonoids, phenolics, steroids, terpenoids, saponins, glycosides, carbohydrates, tannins, and anthraquinones. Both phenolics and flavonoids were mostly abundant, followed by terpenoids, steroids, and tannins.

Table 2 Phytochemical analysis of aqueous extract from *Acacia nilotica* pods

Phytochemical compound	pods extract
Alkaloids	+[a]
Flavonoids	+ + +
Phenolics	+ + + +
Steroids	+ +
Terpenoids	+ +
Saponins	+
Resins	−[b]
Glycosides	+
Carbohydrates	+
Tannins	+ +
Anthraquinones	+

[a] + Present

[b] - Absent

The presence of these active phytoconstituents were similarly explored in extracts of *Acacia nilotica* barks (Arya et al. 2019), pods (Hessien et al. 2022), and leaves (Nkhabindze et al. 2022). They have been reported as reducing, capping, and stabilizing agents in biosynthesis of metal and metal oxides NPs. The capping agent has the potential to decrease the agglomeration and control the growth of particles size, leading eventually to the formation of nano-sized particles (Bawazeer et al. 2021) (Fig. 1).

Owing to their supposed functional properties as reducing agents in NPs synthesis, the phenolic constituents of *Acacia nilotica* extract were further investigated. Figure 2 shows the HPLC-based phenolic fingerprint of major polyphenols at different retention time (RT in minutes). Nine different phenolic compounds were detected, with total phenolic content 365.38 ug/100 g. The presence of these polyphenols was confirmed by comparing their RT with authentic standards. The unknown peaks observed in the chromatogram were characterized as glycosides of flavonols.

Our results are in agreement with those reported by Kaur et al. (2022) from crude extracts of *Acacia nilotica* bark. It is worth mentioning that OH groups present in phenols have the potential to reduce Zn compounds in to ZnO-NPs, as well as capping and stabilizing the formed NPs. Accordingly, separate capping agents are not required in the present synthesis approach. It is hypothesized that the zinc nitrate used can act as a precursor, while the plant extract acts as a reducing and capping agent (Happy et al. 2019).

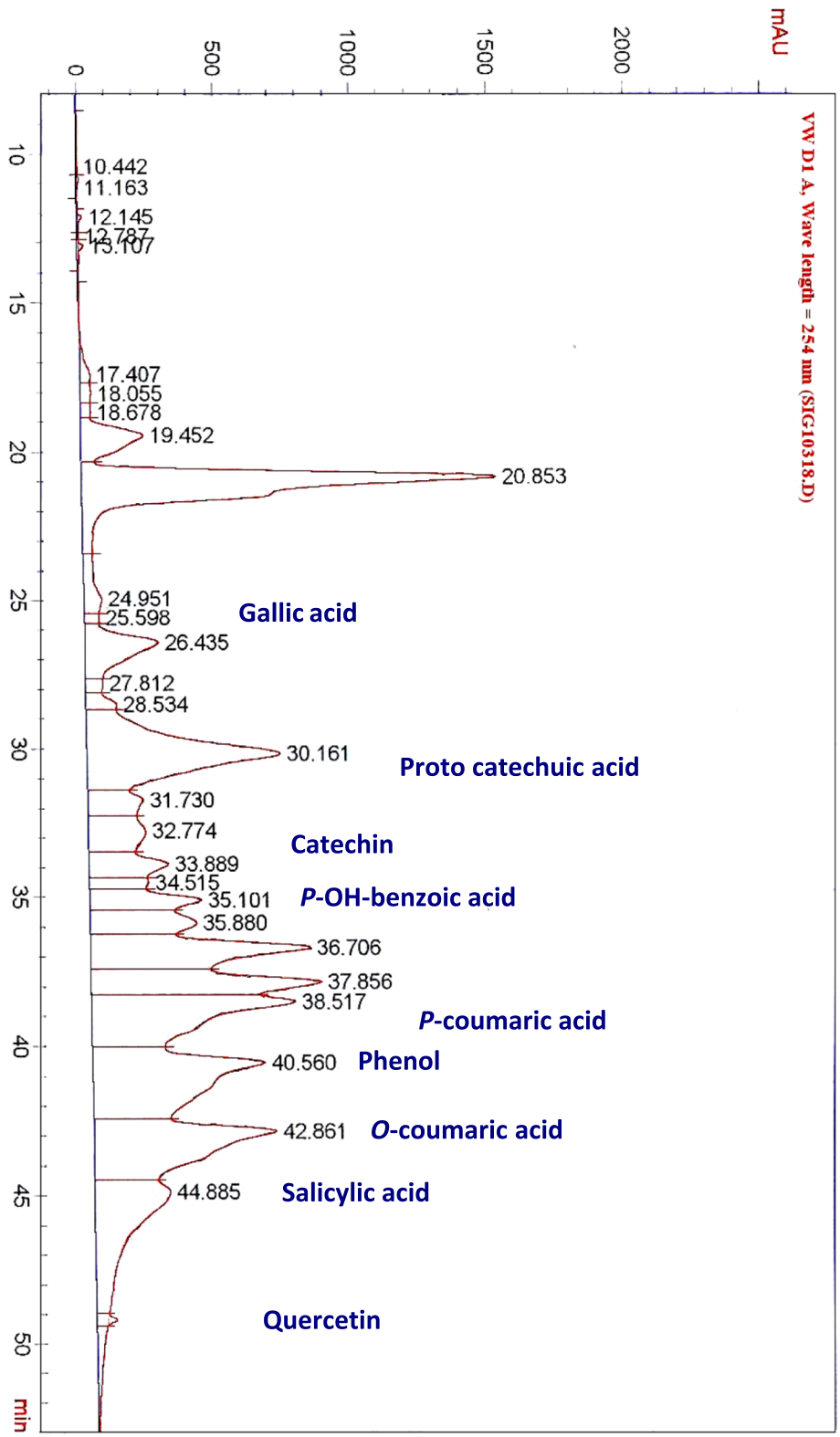

Fig. 1 HPLC of phenolic constituents in *Acacia nilotica*

In vitro antibacterial activity

A comparative inhibition efficiency of both *Acacia nilotica* extract and ZnO-NPs was evaluated against *E. coli* (ATCC 25923) at different concentrations in relation to negative control (sterile distilled water) and positive control (streptomycin standard antibiotic). As evident from Table 3, the diameters of inhibition zones ranged between a mean

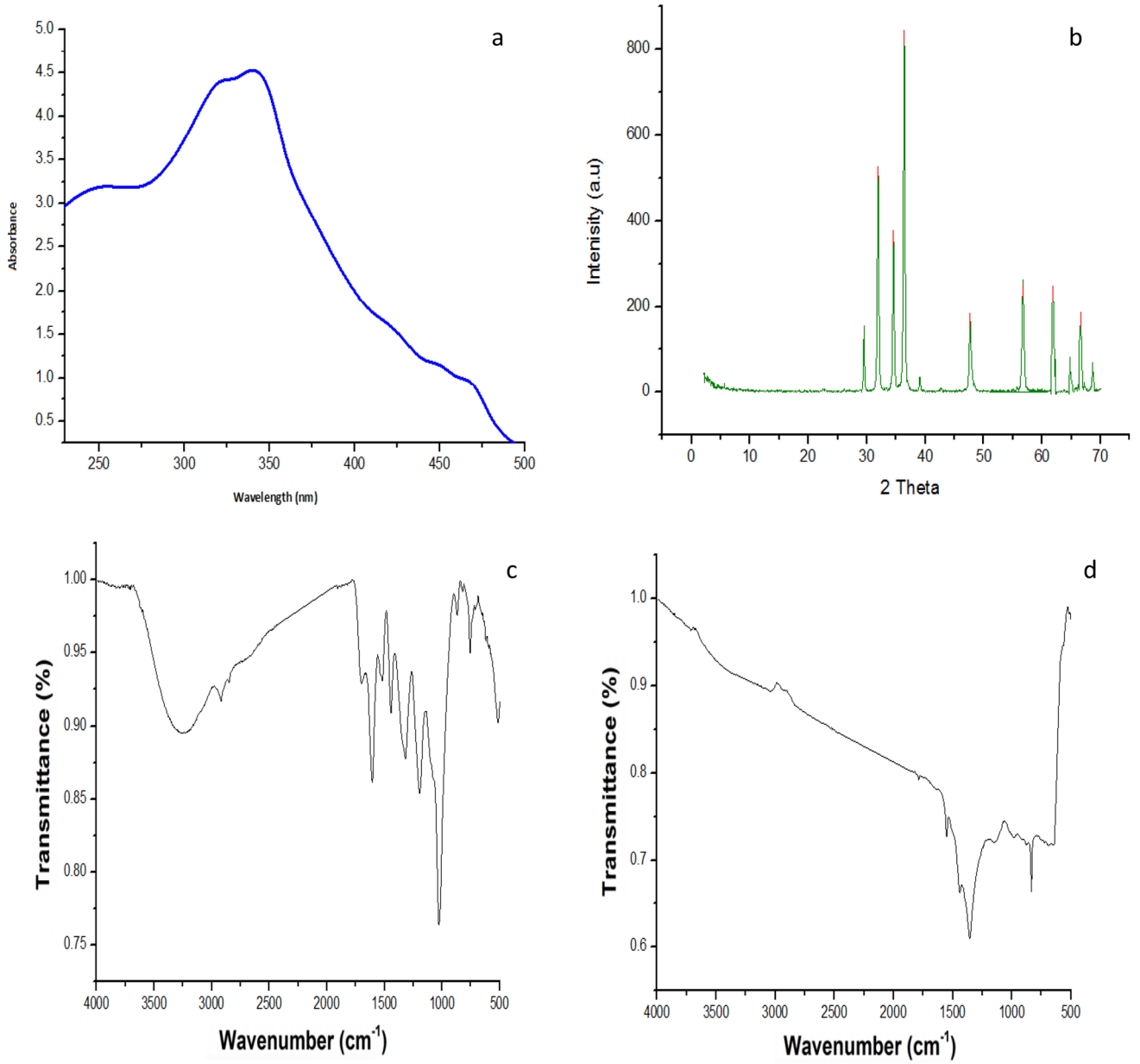

Fig. 2 Optical characterization of phytofabricated ZnO-NPs. **a**: UV–Visible spectrum; **b**: XRD pattern; **c** & **d**: FTIR spectra of *Acacia nilotica* extract and ZnO-NPs

of 11.0 ± 0.9 to 15.0 ± 0.7 mm for the plant extract, while for ZnO-NPs, they ranged between a mean of 13.0 ± 0.8 to 17.0 ± 0.7 mm. The recorded inhibition zones increased in a dose-dependent manner, and after a range of concentrations (100–400 mg/mL), the activity get leveled off with no much further increase. It was observed that the highest bacterial sensitivity was directed to ZnO-NPs, whose potency was equivalent to that of streptomycin (17.0 ± 0.7 mm).

The antibacterial activity of *Acacia nilotica* extracts (pods, leaves, and bark) was reported in a recent study (Abduljawad 2020). This activity is correlated positively with the results of phytochemical analysis obtained in this investigation and revealed the presence of natural active compounds particularly; phenols, flavonoids, terpenoids, steroids, and tannins are known for their bactericidal effect (Hemlata et al. 2020). Our results are in harmony with several studies that confirmed the effectiveness of *Acacia nilotica* extracts against *E. coli* (Hameed et al. 2017; Jame 2018; Kaur et al. 2022). It seems possible that the plant extract not only contributed in the synthesis of the metal oxide NPs, but was also engaged in a synergistic antibacterial action with the nano-zinc oxide. The strong antibacterial

Table 3 Zones of inhibition (mm) of aqueous extract from *Acacia nilotica* pods and phytofabricated ZnO-NPs against *E. coli*

Concentrations (mg/mL)	Zones of inhibition (mm)					
	Acacia nilotica extract			ZnO-NPs		
	Min	Max	Mean ± SE	Min	Max	Mean ± SE
100	9.0	12.0	11.0 ± 0.9	12.0	14.0	13.0 ± 0.8
200	10.0	13.0	12.0 ± 0.8	12.0	15.0	14.0 ± 0.9
300	12.0	14.0	13.0 ± 0.8	14.0	17.0	16.0 ± 1.08
400	13.0	15.0	15.0 ± 0.7	16.0	18.0	17.0 ± 0.7
Control [a]	0.0	0.0	0.0 ± 0.0	0.0	0.0	0.0 ± 0.0
Streptomycin [b]	16.0	18.0	17.0 ± 0.7	16.0	18.0	17.0 ± 0.7

Values are mean inhibition zones (mm) ± standard error of 3 independent replicates

[a]negative control (sterilized distilled water)

[b]positive control (standard antibiotic 30 µg/mL)

activity of ZnO-NPs reported in our study was in accordance to that reported by Pachaiappan et al., (2021) who found that the zone of inhibition radius of ZnO-NPs from zinc nitrate against *E. coli* was 15 ± 0.14 mm compared to that from zinc acetate dehydrate (10 ± 0.1 mm) and zinc sulfate (12 ± 0.3 mm). ZnO-NPs synthesized from extracts of *Acacia nilotica* pods were also found to overcome carbapenem-resistant *Klebsiella pneumonia* (Rasha et al. 2021).

UV–visible spectral characterization

The UV–Vis spectrophotometer technique is usually the premium technique used to assess the structural characteristics of NPs through determining the absorbance of measurement after change in the plant extract color. The appearance of new absorption band confirms NPs formation. As shown in Fig. 2a, the UV–Vis spectrum findings demonstrated that the presence of secondary metabolites in the plant extract has led to a stable synthesis of ZnO-NPs. The *Acacia nilotica* extract not only functions as a reducing agent, but also as a stabilizer. Freshly prepared ZnO suspensions from the plant extract exhibited a strong surface plasmon resonance absorption band around 340 nm in the UV region; meanwhile, the change in color from brown to pale yellow then to white precipitate after adding sodium hydroxide (2 M) was the key indicating the reduction of metal oxide and formation of ZnO-NPs from zinc nitrate. Similar to this finding, a study reported that the UV spectrum range of ZnO-NPs was between 320 and 360 nm using the plant *Bridelia ferruginea* (Gurgur et al. 2020). Our results are well-supported by Vijayakumar et al. (2016) who reported that UV– Vis absorbance spectrum of pure ZnO-NPs was at 338 nm. The same finding was confirmed in another recent study in which zinc nitrate was used as a precursor and the leaves extract of *Justicia adhatoda* as reducing and capping agent (Pachaiappan et al. 2021).

XRD spectral characterization

X-ray diffraction is mainly used for confirming the formation of zero-valent NPs as well as determining their crystalline structure and morphology through comparing the observed diffraction pattern with a reference library. If the NPs are formed in amorphous structure, no diffraction peaks are expected to be obtained (Ettadili et al. 2022). The X-ray diffraction pattern of phytofabricated ZnO-NPs obtained in this study is shown in Fig. 2b. The sharpness of the XRD peaks showed that the synthesized nanomaterial had a good crystalline structure and reflects the effect of capping agents present in *Acacia nilotica* extract. The sample was analyzed at a range of angles from 0° to 100°. The prominent X-ray diffraction peaks exhibited by ZnO-NPs were at $2\theta = 31.923°$, 34.539°, 36.4024°, 39.0701°, 47.6484 and 54.555°,61.525°, 62.365°and 69.05° which could be corresponding to the lattice planes (100), (002), (101), (102), (110), (103), (200), (112) and (201), respectively. The results of XRD pattern confirmed the hexagonal crystalline structure of ZnO-NPs, and that the examined sample was formed completely of zincite (a pure form of ZnO whose crystallographic phase is hexagonal). The XRD pattern is in good agreement with the Joint Committee on Powder Diffraction Standards (JCPDS) data sheet/ICDD with card no 96-230-0113 (Heidrun and Hans 2006). This clearly shows that ZnO-NPs have been successfully formed by phytoassisted green synthesis method. The particle diameter of ZnO-NPs was calculated from the highest peak (101) in the XRD graph according to Debye Scherrer's equation given as follows:

$$d = K\lambda/\beta\cos\theta \quad (5)$$

d: crystallite size; K: constant around unity (0.94); λ: diffraction wavelength; β: corrected FWHM (full width at half maximum) of the peak located at 2 θ; and θ: Bragg's angle of diffraction. The average particle crystallite size (d) of

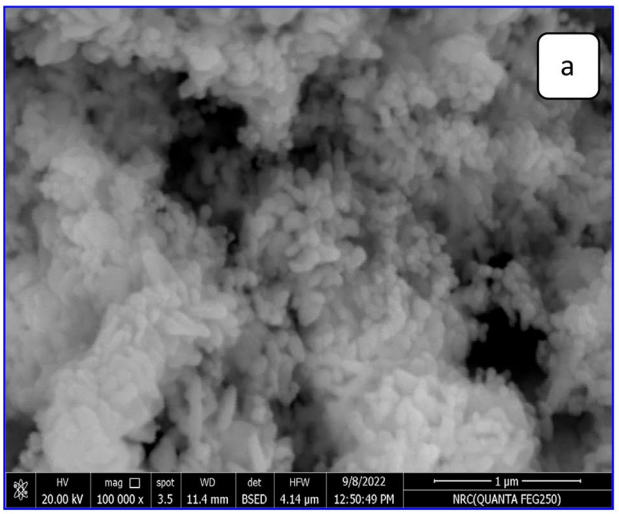

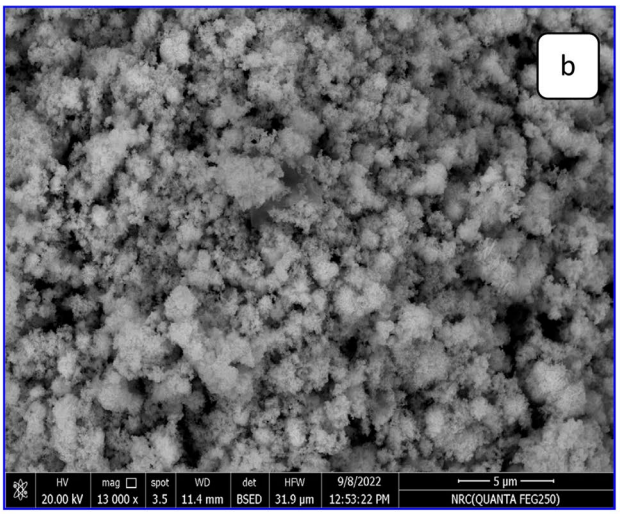

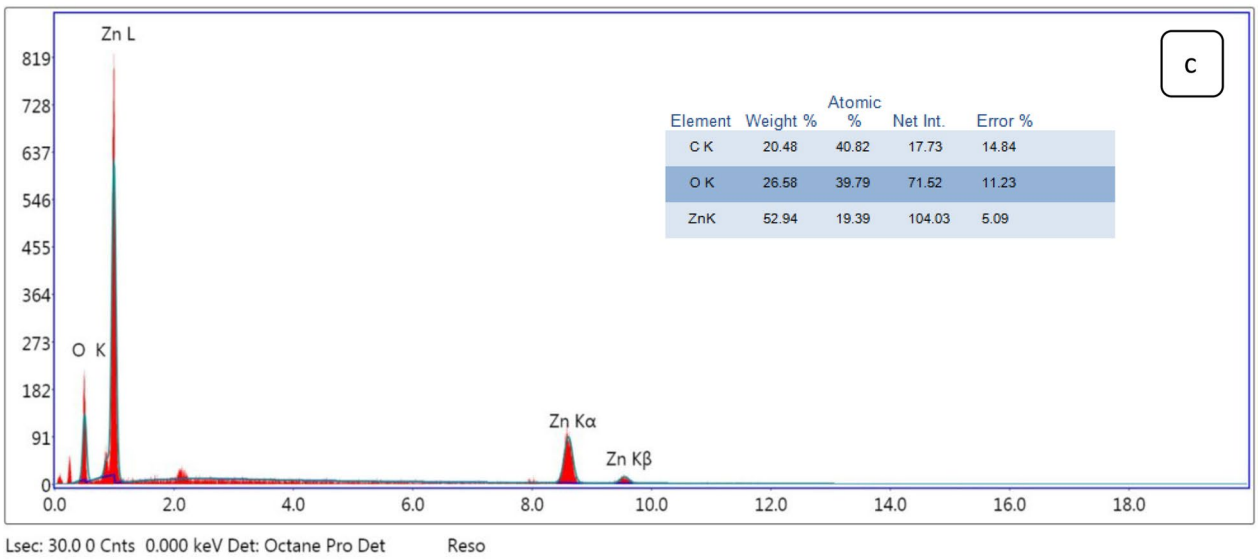

Element	Weight %	Atomic %	Net Int.	Error %
C K	20.48	40.82	17.73	14.84
O K	26.58	39.79	71.52	11.23
ZnK	52.94	19.39	104.03	5.09

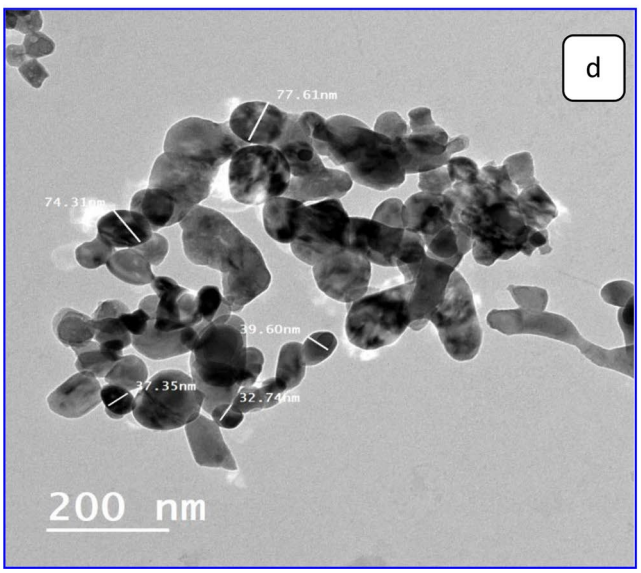

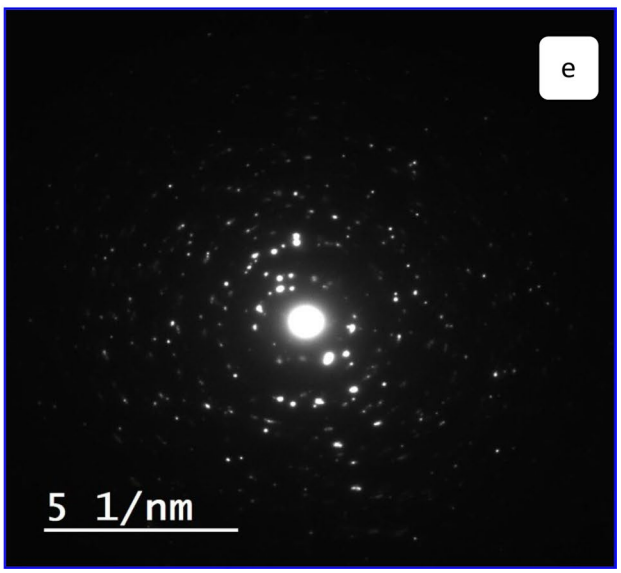

◂**Fig. 3** Morphological characterization of phytofabricated ZnO-NPs. **a** & **b**: SEM images with different magnifications (1 and 5 µm); **c**: EDX analysis; **d** & **e**: TEM images

phytofabricated ZnO-NPs calculated by Scherrer's formula came out to be around 33.87 nm. Our results are on par with recent reports from Mydeen et al. (2020), Umamaheswari et al. (2021), and Hessien et al. (2022).

FTIR spectral characterization

FTIR spectroscopy was applied to determine the major functional groups present in *Acacia nilotica* extract and their possible involvement in the reduction, stabilization, and formation of ZnO-NPs. The FTIR spectra obtained from the aqueous extract of *Acacia nilotica* pods and synthesized ZnO-NPs are demonstrated in Fig. 2c and d, respectively.

As given in Fig. 2c (FTIR of *Acacia nilotica* extract), it showed characteristic absorption bands at different frequencies. At 3257 cm^{-1}, a broad band attributed to O–H alcoholic and phenolic hydroxyl group and or/ carboxylic acid was recognized. The bands appearing at 2918 cm^{-1} and 2850 cm^{-1} indicate the presence of C-H aliphatic hydrocarbon of terpenoids. Meanwhile, the peaks observed at frequencies 1698 cm^{-1}, 1605 cm^{-1}, 1443 cm^{-1}, and 1317 cm^{-1} are characteristic for C = O stretching vibration of carboxylic acid, C = C of olefinic group in terpenoid aromatic ring, C-H bending vibration of aliphatic hydrocarbon, and C-O of phenolic hydroxyl group, respectively (Iravani 2011). The strong absorption band at 1027 cm^{-1} indicates the presence of C–O–C glycoside linkage, while the band at 869 cm^{-1} stands for C-H of olefinic terpenes. The band at 821 cm^{-1} corresponds to C-H bending vibration of para-disubstituted aromatic proton, while bands at 756 cm^{-1} and 712 cm^{-1} are attributed to the bending vibration of ortho- disubstituted aromatic proton.

According to literature, FTIR results of the plant extract confirm the evidence of phenolics, flavonoids, terpenoids, and tannins (Saratale et al. 2019). These results are in complete agreement with those obtained from preliminary phytochemical analysis in this study. The presence of OH group in phenols and flavonoids plays a major role in NPs formation through reduction in the metal ions; meanwhile, terpenoids are responsible for the oxidation of aldehydes in to carboxylic acid, thus causing reduction in the metal ions. It seems that both flavonoids and terpenoids induce reduction in metal ions into stabilized NPs by active chelation. This was proved due to appearance of the peak obtained for carbonyl groups. The reduction in metal ions into NPs is assumed to be through the release of reactive hydrogen atom from enol-form to the keto-form as a result of tautomeric transformations of flavonoids (Umamaheswari et al. 2021).

When FTIR spectra of the plant extract and ZnO-NPs were compared, the spectra showed different IR absorption. As shown in Fig. 2d (FTIR of ZnO-NPs), the peaks related to the plant extract either decreased or even disappeared, which indicates that these functional groups were mainly involved in the reduction and stabilization of ZnO-NPs. The suppression in intensity or disappearance of bands at frequencies 3257, 2918, 2850, 1698, 1605, 1027, and 712 cm^{-1} indicates the involvement of carboxylic acid, alcohol, glycoside, phenols, and carbonyl moieties with ZnO-NPs synthesis and stabilization (Sohail et al.2020). On the other hand, the intense band at 1551 cm^{-1} depicts the presence of C = C stretching vibration of aromatic groups (Vijayakumar et al.2018), and the band at 1355 cm^{-1} corresponds to C–O–H bending mode (Sundrarajan et al.2015). The band at 1151 cm^{-1} can be attributed to the characteristic absorption of C-O vibration; meanwhile, the strong absorption band at 834 cm^{-1} is indicative to the presence of C-H bending of aromatic protons (Vijayakumar et al.2018). The sharp band for Zn–O stretch appeared below 500 cm^{-1}, having weak bands positioned at 513, 482, 466, 436 cm^{-1}, and two strong bands at 418 and 413 cm^{-1} ascribed to the presence of ZnO-NPs (Elumalai et al., 2015; Verma and Mehata 2016).

SEM and EDX analysis

SEM images at different magnifications (1 and 5 µm) coupled with EDX analyses were used to confirm the presence of phytofabricated ZnO-NPs and elucidate their elemental composition, shape and size. As shown in Fig. 3a, the image at magnification 1 µm showed that the surface of ZnO-NPs was almost completely colonized by numerous *E. coli* cells, of which some cells were buried in between the NPs gaps. In Fig. 3b, the image at magnification 5 µm showed that the ZnO-NPs were mostly presented in hexagonal shape with some spherical irregular shaped and aggregated NPs. The average particles diameter was found to be around 33.43 nm, which corresponds to the XRD result (33.87 nm). Our results are in agreement with those previously reported for ZnO-NPs prepared from *Acacia nilotica* pods extract and showed hexagonal-shaped NPs with smooth surface free of cracks (Rasha et al. 2021). Another study showed that ZnO-NPs prepared from *Justicia adhatoda* leaves extract exhibited agglomerated morphology with cubic shape when zinc nitrate was used as a precursor and was orthogonal/ nanorod when zinc sulfate was the precursor. The differences in shape and morphology of phytofabricated NPs could be attributed to differences in precursors and capping agents (plant extract) used (Pachaiappan et al. 2021).

The EDX spectrum of ZnO-NPs shown in Fig. 3c shows emission of strong signals of zinc and oxygen elements, confirming that ZnO-NPs are essentially free from impurities, and it is seen in the limit of the EDX. The elemental analysis

revealed the presence of 52.94% zinc and 26.58% oxygen, indicating that the synthesized NPs are of high purity and quality. The presence of carbon (20.48%) in the EDX spectrum could be related to bioactive compounds originated from the plant extract. The amount of oxygen present indicates that the plant phytochemical groups are involved in the reduction of zinc ions, capping, and stability of the formed zinc oxide NPs (Gupta et al. 2018).

TEM analysis

The transmission electron microscopy technique is known for its high magnification and resolution power by which we can study the morphology and mean size of synthesized NPs ranging between 1 and 100 nm. It can also distinguish crystalline structure from amorphous one, thus confirming results obtained from XRD and SEM analysis (Sheny et al. 2011). As presented in Fig. 3d, the TEM image revealed that the green synthesized ZnO-NPs were polycrystalline with the majority hexagonal in structure and few spherical aggregated NPs. The selected area electron diffraction image in Fig. 3e reflected the presence of concentric rings which approves the crystalline nature of formed NPs. The average particles size drawn from the TEM analysis was about 32.74 nm. Larger NPs sizes of an average 77 nm were also recorded; meanwhile, very small NPs of about 9 nm were also observed. The small-sized NPs possibly reflect the high reducing efficacy and capping ability of phytochemicals present in *Acacia nilotica* leaf extract (Singh et al. 2019).

The TEM results are in good agreement with those obtained from both XRD and SEM analysis, and also match with those reported from Hessien et al. (2022) who obtained ZnO-NPs of crystal size 13 nm and Rasha et al. (2021) in which the TEM analysis showed similar NPs size ranging from 16 to 90 nm.

Adhesion capacity, kinetics, and isotherm studies

The adhesion capacity of *E. coli* (ATCC 25923) onto ZnO-NPs at different time intervals (15–120 min) was studied. As shown in Fig. 4a, the adhesion rate increased rapidly within the first 60 min and then slowed down gradually till it reached equilibrium after 120 min at which the maximum adhesion capacity achieved was 464×10^7 cfu g^{-1} using 0.5 g of phytofabricated ZnO-NPs. The adhesion capacity increased about 1.7-folds by increasing the contact time from 15 to 120 min. The above results demonstrate the high potential of ZnO-NPs to capture *E. coli* cells from aqueous solutions thus promoting their removal.

Several kinetic models were applied to investigate the adhesion mechanism and removal of *E. coli* from aqueous solutions to different NPs. Herein, explanations based on correlation between our experimental data and kinetic models were developed using the pseudo-first- and second-order kinetics, being the most simple and applicable models (Fan et al., 2017). Equations (6) and (7) are used to express both, respectively, as follows:

$$\mathrm{Log}\left([\mathrm{surf}] - \left[\mathrm{surf_t}\right]\right) = \log[\mathrm{surf}] - K_1 t/2.303 \tag{6}$$

$$t/\left[\mathrm{surf_t}\right] = 1/(k_2[\mathrm{surf}]^2 + t/[\mathrm{surf}] \tag{7}$$

[surf] represents the *E. coli* adhesion at equilibrium, while [$surf_t$] represents the *E. coli* adhesion at different time intervals. As given in Table 4 (I) and Fig. 4b and c, the values of pseudo-first-order rate constant (k_1), the pseudo-second-order rate constant (k_2), and the theoretical adhesion capacity [surf] at equilibrium were determined from the slopes and the intercepts of the plots of log ([surf]− [$surf_t$]) and t/[$surf_t$] against the time. The obtained data revealed that the regression correlation coefficient (R^2) for the pseudo-second-order model was higher (0.992) than that in the pseudo-first-order model (0.910), and the fitting of the kinetics data showed excellent linearity. Also, the calculated [surf] value (5.02) obtained when applying the pseudo-second-order model was well-matching with data (4.66) obtained from experimental adhesion studies. Accordingly, the pseudo-second-order kinetics is best fit for describing the adhesion mechanism of *E. coli* to ZnO-NPs. This indicates that the electrostatic interaction between the *E. coli* cells and the ZnO-NPs was the key driving force in the adhesion process. In a similar study, the adhesion equilibrium of *E. coli* cells to zinc oxide coated with zeolite was best described through pseudo-second-order model, and the adhesion rate was predicted to be directly proportional to square the concentration of *E. coli* cells and the number of the active sites present on the zinc oxide particles (Wang et al. 2018). Our results were also in harmony with those reported in a study investigating the removal of waterborne *Staphylococcus aureus* using zinc oxide-coated zeolite. The study showed that the electrostatic attraction force could ensure a strong adhesion as well as inhibition of *Staphylococcus aureus* release from the zinc oxide particles bearing positive charges (Wang et al. 2019).

The linear regression analysis is considered a premium tool that can describe well the adhesion process isotherm. In the present investigation, Langmuir and Freundlich isotherms have been applied (Foo and Hameed 2010). The Langmuir isotherm assumes that the adhesion is monolayer and that it takes place at certain homogeneous sites on the adsorbent. No further adsorption can occur when the sites are fully occupied with adsorbate. It is expressed as follows:

$$\frac{1}{[\mathrm{surf}]} = \frac{1}{\left[\mathrm{surf_{max}}\right]} + \left(\frac{1}{\left[\mathrm{surf_{max}}\right]K_L}\right)\left(\frac{1}{\mathrm{Bulk}}\right) \tag{8}$$

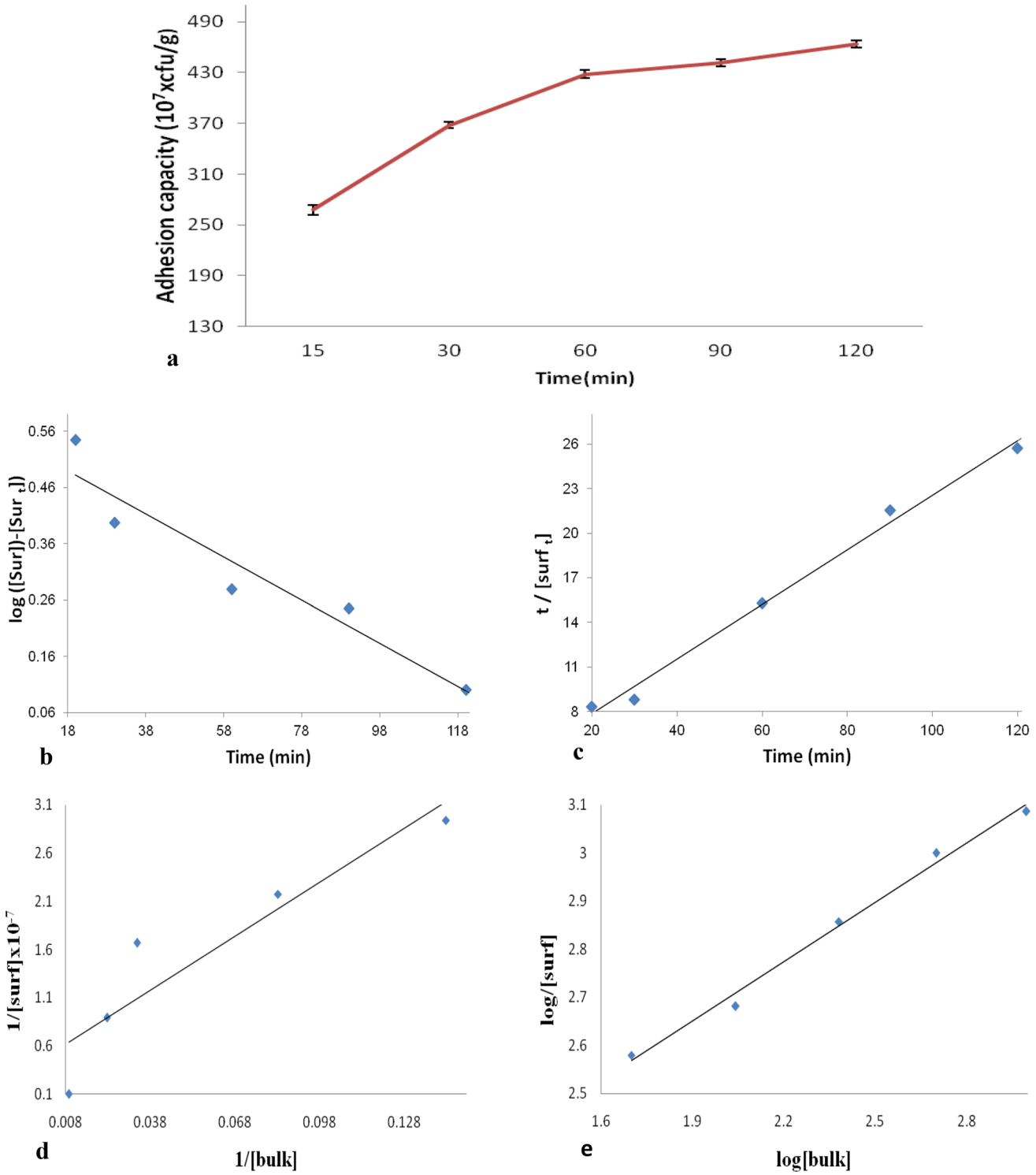

Fig. 4 Fitted plots of Kinetic and isotherm models describing *E. coli* adhesion onto ZnO-NPs. **a**: Adhesion capacity; **b**: Pseudo-first-order model; **c**: Pseudo-second-order model; **d**: Langmuir isotherm; **e** Freundlich isotherm

The term [Surf] refers to the adhesion capacity of *E. coli* at equilibrium at different cells concentrations. [$surf_{max}$] represents the saturation capacity of monolayer adhesion (cfu g^{-1}), K_L denotes to the Langmuir affinity constant for *E. coli* adhesion to nano-ZnO surface, and [Bulk] represents the residual *E. coli* concentration at state of equilibrium. By plotting the relationship between 1/ [surf] and 1/ [Bulk], we can determine the values of [$surf_{max}$] and K_L from the

Table 4 Kinetic and isotherm parameters for adhesion of *E.coli* onto ZnO-NP

(I)					
Pseudo-first order			Pseudo-second order		
[surf], calc. (cfu g^{-1})	K_1 (min^{-1})	R^2	[$surf_t$], calc. (cfu g^{-1})	K_2 (g cfu $^{-1}$ min^{-1})	R^2
3.6	0.011	0.910	5.02	0.007	0.992
(Π)					
Langmuir			Freundlich		
[$surf_{max}$](cfu g^{-1})	K_L	R^2	K_F	n	R^2
1.15	0.05	0.930	19.1	2.4	0.990

(I) Pseudo-first and second-order kinetics

(Π) Langmuir and Freundlich isotherms

intercept and the slope of the plots, respectively (Fig. 4d). The isotherm parameters obtained from fitting the Langmuir model are given in Table 4 (Π).

The Freundlich isotherm is an empirical formula employed for describing the multilayer adhesion over a heterogeneous surface (Yadav and Singh 2017). The linearized form of this isotherm is expressed by the following equation:

$$\log [surf] = \log K_F + n \log [Bulk] \quad (9)$$

The Freundlich constant (K_F) indicates the adhesion capacity and n is the heterogeneity factor related to the adhesion intensity of *E. coli* cells to the surface of nano-ZnO. The values of K_F and n were determined from the slope and the intercept of the plot of log [surf] against log [Bulk] as shown in Fig. 4e. The isotherm parameters obtained from fitting the Freundlich model are given in Table 4 (Π). Comparing the R^2 values, it was found that the correlation coefficient (R^2) of the Langmuir model was 0.930, while the R^2 value of the Freundlich plot (0.990) was close to unity at 22 °C. This indicates that the Langmuir model did not fit well to explain the process of adhesion; meanwhile, the Freundlich isotherm model was better fitted. Previous studies have also shown that the bacterial adhesion to NPs can be evaluated based on particles size, where the maximum removal efficiencies were achieved using the smallest size for nanomaterials (Hooshyari 2017). The K_F value (19.1) obtained in this study indicates a high attachment of *E. coli* to the zinc oxide NPs. Concerning the Freundlich adsorption intensity ($n = 2.4$), it can be used to predict the nature of the adsorption process. Values < 1 indicates that the process was governed by a chemical mechanism; meanwhile, values > 1 implies that the adhesion was governed by a physical process.

Response surface methodology (RSM)

The Box–Behnken design under RSM was employed to design the experiments which investigate the interaction between the different independent variables with the aim of optimizing the adhesion process and removal of *E.coli* from wastewater. According to the Box–Behnken design, 17 runs were carried out, and both actual and predicted responses (*E.coli* removal percentages) are shown in Table 5. Following RSM results, the multiple regression analysis for *E.coli* adhesion and removal was obtained according to the second-order polynomial Eq. (10) as follows:

$$\begin{aligned}&\text{The predicted value of } E.coli \text{ removal}(\%)\\ &= 84.636 + 9.29125 * A + -12.7363 * B + 3.055 * C\\ &\quad + -5.60 * AB + -2.2175 * AC + 0.2025 * BC\\ &\quad + -2.728 * A^2 + -12.313 * B^2 + 5.3695 * C^2\end{aligned} \quad (10)$$

Equation (10) clearly shows how the individual variables and the interaction between two variables can influence *E.coli* adhesion and removal either positively or negatively. A variable positive impact reflects the improvement in the desired response (adhesion) when the variable level increases, while a variable negative impact indicates no improvement in the response along with increasing the variable level (Jafari et al. 2016). According to Eq. (10), the factors (A and C) had positive effects on the adhesion process; meanwhile, the factor (B) had negative effect. In line with the previous findings, increasing the disinfectant dose (A) and the contact time (C) resulted in increasing the adhesion efficiency and *E.coli* removal percentage. On the contrary, increasing the initial concentration of *E.coli* resulted in decrease in the removal efficiency. Also, the highest coefficient related to the disinfectant dose confirms that this variable exerted the optimum effect when compared to the other two variables. Our findings are in agreement with those reporting the maximum significant relationship between the dose of silver-coated $Ni_{0.5}Zn_{0.5}Fe_{0.5}$ magnetic nanocomposite (disinfectant) and *E.coli* inactivation in water (Asadi and Moeinpour 2019).

Table 5 Experimental design for three independent variables based on BBD

Run	Factor 1 (A) Disinfectant dose (g/L)	Factor 2 (B) *E. coli* concentration (cfu/mL)	Factor 3 (C) Contact time (hours)	*E. coli* removal (%) Actual value	Predicted value
1	1	0	1	93.11	91.18
2	0	0	0	97.80	98.32
3	0	1	1	98.10	99.48
4	−1	0	−1	69.10	71.03
5	1	1	0	99.70	100
6	0	0	0	99.80	98.32
7	0	0	0	97.60	98.32
8	0	0	0	98.90	98.32
9	0	1	−1	98.40	97.02
10	0	0	0	97.50	98.32
11	−1	−1	0	69.10	68.55
12	0	−1	−1	89.50	88.12
13	1	0	−1	97.10	97.92
14	−1	0	1	77.40	76.58
15	−1	1	0	87.40	86.85
16	0	−1	1	84.10	85.48
17	1	−1	0	96.10	96.65

Analysis of variance (ANOVA)

The model significance and data adequacy were evaluated using *F*- and *P*-values of ANOVA at 95% confidence level, and the results are presented as given in Table 6. *F*-value (72.19) and *P*-value (< 0.05) for the F-test of the model indicated that the quadratic polynomial equation was statistically significant and can be used for prediction of *E.coli* removal

Table 6 ANOVA regression model for *E. coli* removal

Source	Sum of squares	df	Mean sum of square	*F*-value	*P*-value
Model	2981.80	9	331.31	72.19	< 0.0001
A	690.62	1	690.62	150.48	< 0.0001
B	1297.70	1	1297.70	282.76	< 0.0001
C	74.66	1	74.66	16.27	0.0050
$A \times B$	125.44	1	125.44	27.33	0.0012
$A \times C$	19.67	1	19.67	4.29	0.0772
$B \times C$	0.1640	1	0.1640	0.0357	0.8554
A^2	31.33	1	31.33	6.83	0.0348
B^2	638.36	1	638.36	139.09	< 0.0001
C^2	121.40	1	121.40	26.45	0.0013
Residual	32.13	7	4.59		
Lack-of-fit	22.05	3	7.35	2.92	0.1639
Pure Error	10.08	4	2.52		
Cor Total	3013.92	16			
Std. Dev	2.14	R^2			0.9893
Mean	80.08	Adjusted R^2			0.9756
C.V. %	2.68	Predicted R^2			0.8777
		Adequate Precision			26.9246

A disinfectant dose

B Initial *E. coli* concentration

C contact time

df degree of freedom

from wastewater (Jadhav et al 2013). The ANOVA analysis revealed that the linear (*A*, *B*, *C*), the square (A^2, B^2, C^2), and the interaction effect (AB) were statistically significant in which their P-values were less than 0.05. Meanwhile, the high P-values (greater than 0.05) of AC (0.0772) and BC (0.8554) were indicative of the insignificant role of these terms in the adhesion and removal of *E.coli* by ZnO-NPs.

The lack-of-fit was insignificant (*P*-value = 0.163) indicating that the model was valid and significant to explain the adhesion process (Jafari et al. 2016). The fit of the model was also evaluated for validity by the determination coefficient (R^2) that ranges between 0 and 1, and when it is closer to 1, the model is considered stronger. The high value of the determination coefficient ($R^2 = 0.9893$) revealed a good correlation between the actual and predicted response (Fig. 5a). The determination coefficient (R^2) indicated that about 98.9% of the total variations in *E.coli* adhesion could be explained by the above estimated model, and only less than 2% of the total variables could not be described. The adjusted R^2 and the predicted R^2 also confirmed the model significance for describing the adhesion process of *E.coli*. Adjusted R^2 (0.9756) close to R^2 confirmed the good correlation between the required response (adhesion) and the fitted model. Predicted R^2 (0.8777) revealed that the predicted response was well-estimated through the applied model.

As shown in Table 6, the R^2, the adjusted R^2, and the predicted R^2 are not significantly different from each other. On the other hand, the adequate precision measures the signal-to-noise ratio in which a ratio greater than 4 is considered desirable. In the present study, this ratio was found to be 26.9 which indicate an adequate signal (Jafari et al. 2016). The coefficient of variance (CV %) describes the model reproducibility. Low CV % indicates low deviation between the experimental (actual) and the predicted values. CV % obtained through this study (2.68%) was relatively low (< 10%), thus indicating the model reliability.

The Box–Cox diagram was used for the model verification. To enhance model validity, Lambda (λ) value is commonly used to predict the probable alteration of the experimental values As shown in Fig. 5b, the best lambda value ($\lambda = 1.71$) was obtained between the two red vertical lines, so no data transformation was required. The red line showed the minimum (−0.068) and maximum (4.99) values, as well as λ at 95% confidence level. The current point of confidence interval ($k = 1$) matched with the model design value (best = 1); therefore, no transformation of the model was required as recommended by the Box–Cox analysis.

Interactive effects of operating variables

The response surface (3D) plots for the removal percentages of *E.coli* versus the interactive effects of disinfectant dose, initial *E.coli* concentration, and contact time are illustrated in Fig. 6. Each plot displays the percentages of removal efficiency (response) on the Z-axis and two of the test variables on the X- and Y- axes while maintaining the other variable at the zero level (central point).

Figure 6a shows the effect of the interaction of ZnO-NPs dose disinfectant and the contact time on the removal of *E.coli* from the aqueous solution. It can be seen that as the

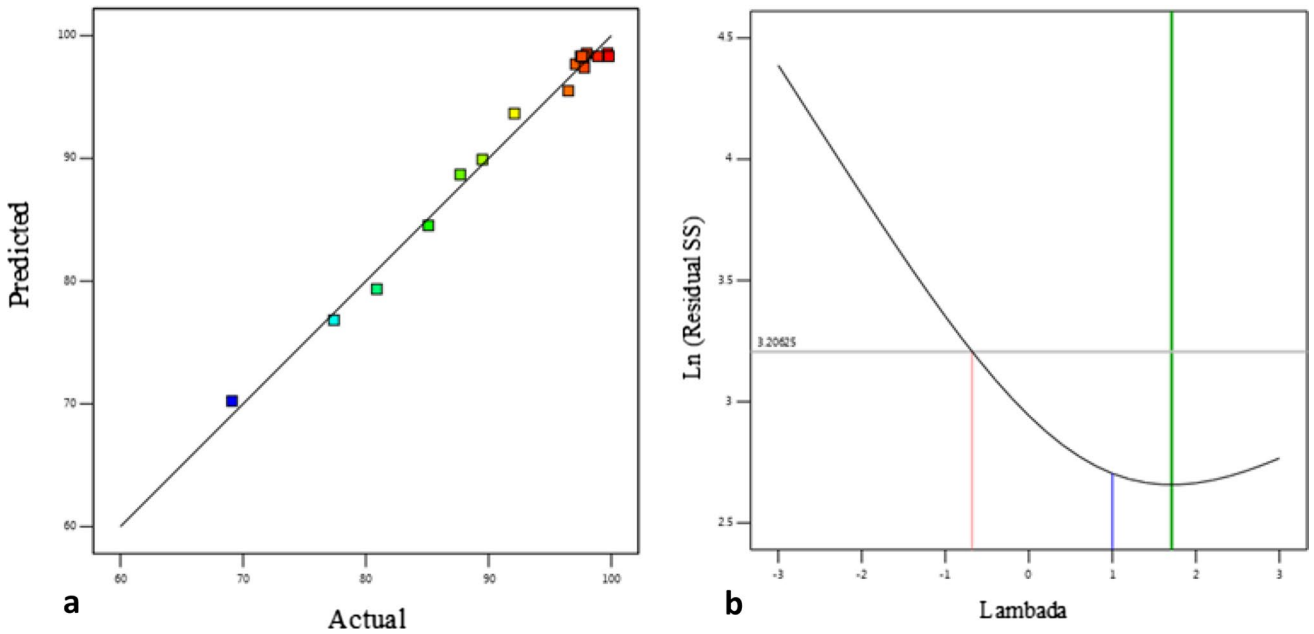

Fig. 5 Plot of predicted versus actual values of *E.coli* removal by ZnO **a** and **b** Box–Cox plot of model transformation

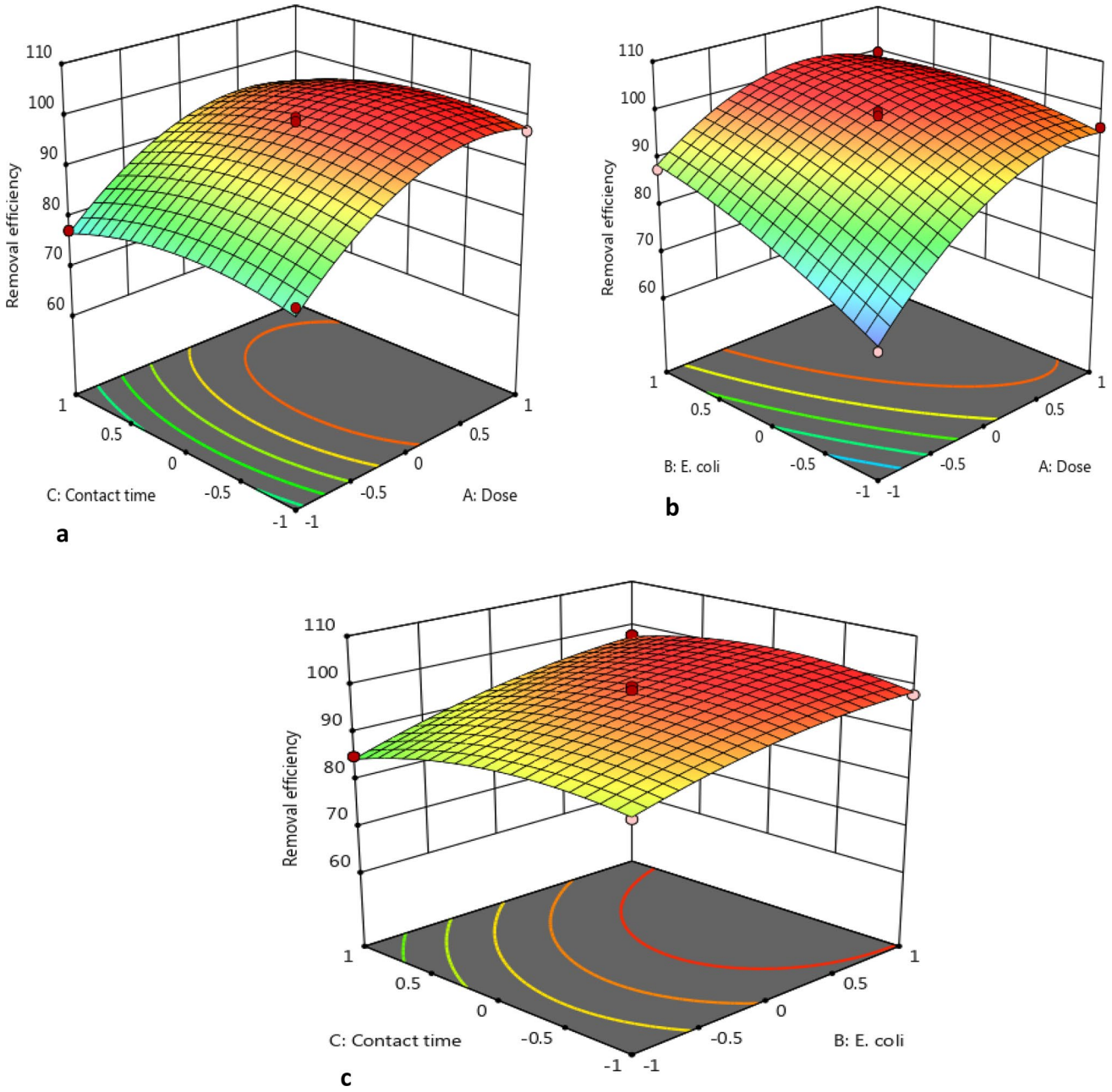

Fig. 6 Response surface plots demonstrating the variations in *E.coli* removal efficiency (%) as a function of: **a** contact time and disinfectant dose; **b** *E.coli* concentration and disinfectant dose; **c** contact time and *E.coli* concentration

dose of ZnO-NPs increased, the removal efficiency increased until reaching equilibrium. The observed trend can be explained by the fact that the dosage of ZnO-NPs increased the number of adhesion sites available to speed up the initial contact with *E.coli* cells, leading to more *E.coli* collision on the ZnO-NPs surface and enhancing the adhesion process. The percentage of *E.coli* removed is decreased over a longer period of time as *E.coli* cells occupied all of the available vacant sites on the ZnO-NPs.

Figure 6b demonstrates the combined impact of ZnO-NPs dose and the initial *E.coli* concentration on *E.coli* elimination. It should be observed that the *E.coli* removal increased with increasing ZnO-NPs dose and decreasing *E.coli* concentration. This is due to the fact that as the initial *E.coli* concentrations increase gradually, the adhesion sites on the ZnO-NPs become also saturated gradually, resulting in decrease in the adhesion efficiency.

Figure 6c reveals the interactive effect of initial *E.coli* concentration and contact time on the removal of *E. coli*. The removal efficiency increased first with the increase in contact time duration and then decreased with increasing initial *E.coli* concentration. This is because at low *E.coli* concentrations, the ratio of surface active sites to all *E.coli* cells is high, so all available cells adhere to the ZnO-NPs surface. However, at higher concentrations of *E.coli,* the sites available for adhesion become limited until the process reach the saturation state. Accordingly, the removal efficiency becomes remarkably hampered even if the contact time is increased. In this context, Mostafaii et al (2017) concluded that when the reaction time is increased, the ZnO-NPs could have more time to penetrate the bacterial cell and destruct the cell membrane; hence, the percentage of eliminated bacteria increases. The aggregation of ZnO-NPs in the cell membrane and cytoplasm of the bacteria can inactive them, thus inducing bacterial growth inhibition. In this regard, the nanosize of the ZnO particles makes the bacterial cell membrane piercing easier. Furthermore, the increase in contact time between ZnO-NPs and bacterial cells is accompanied by increase in H_2O_2 production which subsequently intensifies the percentage of eliminated bacteria (Zhang et al. 2007; Asadi and Moeinpour 2019.

Model validation and variables optimization for *E. coli* adhesion

In order to validate the optimum combinations of variables, several confirmatory experiments were carried out. When the command was given to maximize the targeted response (*E.coli* adhesion and removal percentage), a number of combinations along with their responses were predicted as the solution. Few of such combinations were chosen and the confirmatory experiments were run in triplicates. According to the results obtained from RSM using BBD, the best *E.coli* adhesion obtained was 99.8%. This removal percentage was achieved at a disinfectant dose 30 g/L, initial *E.coli* concentration 150×10^7 cfu/mL, and contact time 6 h. The obtained results confirm that RSM was a feasible tool for optimizing the operational conditions needed for optimum adhesion of *E.coli* onto ZnO-NPs and their subsequent removal from wastewater.

Application and reusability of ZnO-NPs for removal of bacteria from wastewater

Wastewater samples obtained from El-Rahawy drain, Giza governorate, Egypt, were analyzed for basic indicators of microbial water pollution. The preliminary screening results revealed an average microbial load of $70\times10^3\pm0.8$, $30\times10^3\pm0.5$, and $17\times10^3\pm0.3$ cfu/100 mL for total coliforms, fecal coliforms, and *E. coli*, respectively.

Application of phytofabricated ZnO-NPs immobilized into sodium alginate beads to real wastewater showed a recognizable disinfection potential. Figure 7 demonstrates the bar chart showing the removal efficiencies in relation to exposure time intervals (1, 3, 6, and 24 h). After 6 h of treatment, the average removal percentages reached $98.2\pm0.6\%$, $97.2\pm0.4\%$, and $96.5\pm0.3\%$ for total coliforms, fecal coliforms, and *E. coli*, respectively. After 24 h, complete

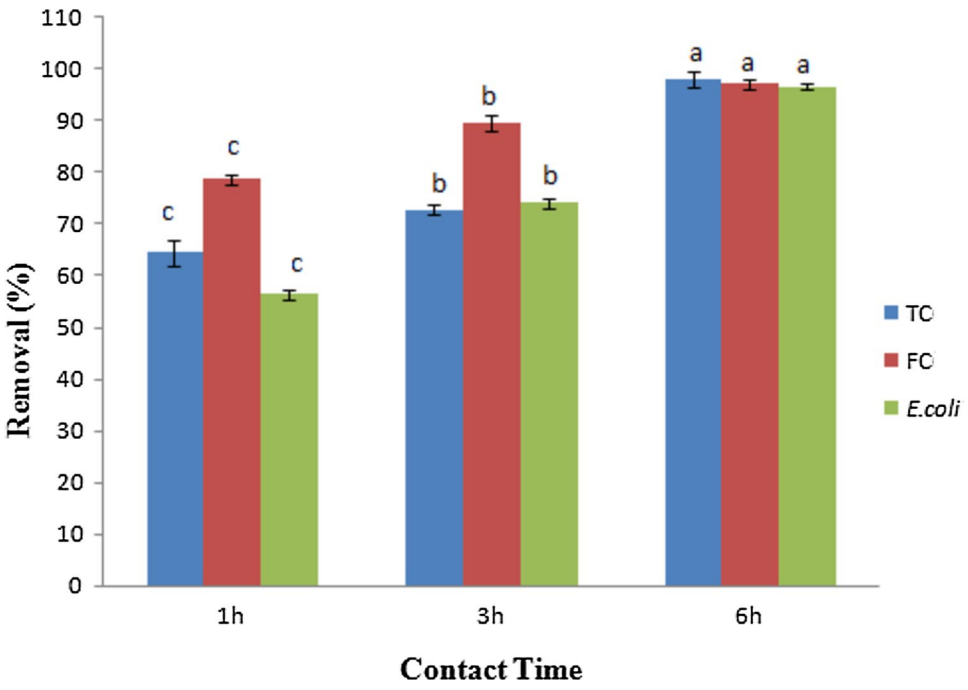

Fig. 7 Removal efficiency of bacteria versus contact time using immobilized phytofabricated ZnO-NPs. TC: total coliforms; FC: fecal coliforms; *E.coli*: *Escherichia coli*. Data are expressed as mean ± SE of three replicate tests and columns with different letters indicate significant differences at $p<0.05$

removal (100%) was achieved. The net average concentrations for the same indicators in the same order recorded 1200 ± 0.8, 850 ± 0.7, and 600 ± 0.4 cfu/100 mL. In this context, the above concentrations fulfill the permissible levels recommended by the World Health Organization (WHO 2006) regarding wastewater reuse in unrestricted irrigation (fecal coliforms and *E. coli* should be ≤ 1000 cfu/100 mL).

The disinfection potential exhibited by ZnO-NPs is supported by our earlier results of in vitro antibacterial activity (Table 3) and correlated well with those of Wang et al. (2018) who reported a removal capacity of *E. coli* from water by zinc oxide impregnated zeolite of about 4.34×10^6 cfu/g. Another study showed the use of zinc oxide nanomaterial to be promising for water and wastewater disinfection and recommended it as cost-competitive antimicrobial that could be incorporated with other conventional water treatment methods (Dimapilis et al. 2018). In a similar study, the effect of zinc oxide nanoparticles was tested on some Gram-negative and Gram-positive bacterial strains (*Escherichia coli* and *Staphylococcus aureus*) and the yeast *Candida albicans*. The study concluded the possibility of successful application of ZnO-NPs in water purification (Spoiala et al. 2021).

Recently, green synthesis of ZnO-NPs from areca nut demonstrated high efficiency against *E. coli* associated with biofilm formation. The authors recommended the use of nano-zinc oxide in wastewater treatment (Raghavendra et al. 2022). Another recent study reported higher potential for zinc oxide decorated with silver nanoparticles used for disinfection of contaminated water from a lake located in the city of Guarapuava, Brazil. The best performance was obtained using 0.5 g of the nanocomposite and could eliminate total coliforms and *E. coli* completely within 15 min of application (Primo et al. 2022).

In the present study, the reusability of immobilized phytofabricated ZnO-NPs was further investigated to elucidate the possibility of *E. coli* removal from real wastewater for several consecutive cycles of treatment using the same precursor NPs. As presented in Table 7, the immobilized nano-zinc showed sustainable efficiency in removing *E. coli* for four consecutive cycles of reuse. The removal percentages reached 96.3 ± 0.8% in the first cycle after 6 h, 95.2 ± 0.4% in the second cycle after 8 h, 94.7 ± 0.3% in the third cycle, and 91.8 ± 0.5% in the fourth cycle after 12 h of treatment. *E. coli* was completely removed (100%) within 24 h. It is worth mentioning that the target *E. coli* load needed for unrestricted irrigation (≤ 1000 cfu/100 mL) was achieved after contact time 6 h in the first cycle (680 ± 0.4 cfu/100 mL), 8 h in the second cycle (750 ± 0.6 cfu/100 mL), and 12 h in the third and fourth cycles (860 ± 0.7 cfu/100 mL and 970 ± 0.8 cfu/100 mL, respectively).The disinfectant reusability is considered an additional advantage favoring the economic feasibility of the treatment process as well as possibilities of large scale applications.

Table 7 Reusability potential of immobilized phytofabricated ZnO-NPs for removal of *E.coli* from wastewater

Removal percentages (%)				
No. of cycles	After 6 h	After 8 h	After 12 h	After 24 h
First cycle	96.3 ± 0.8	98.6 ± 0.2	99.2 ± 0.6	100 ± 0.0
Second cycle	82.5 ± 0.5	95.2 ± 0.4	98.8 ± 0.9	100 ± 0.0
Third cycle	75.8 ± 0.7	86.8 ± 0.7	94.7 ± 0.3	100 ± 0.0
Fourth cycle	60.4 ± 0.3	75.6 ± 0.5	91.8 ± 0.5	100 ± 0.0

Data were expressed as mean ± SE of three replicate tests

Disinfection mechanism

Overall, the proposed mechanism suggested for disinfection of wastewater and *E. coli* removal using ZnO-NPs phytofabricated by aqueous extract of *Acacia nilotica* pods can be summarized as follows (Fig. 8). The first step involves electrostatic interaction between the negatively charged *E. coli* cells and the positively charged ZnO-NPs, thus decreasing the stability of the cells suspension and increasing their adhesion and removal efficiency. The adhesion is characterized by forming a multilayer of *E. coli* cells over heterogeneous active sites on nano-ZnO surfaces. Following this physical interaction, the second step is governed by the strong antibacterial activity of phytofabricated ZnO-NPs in which three mechanisms are suggested (Dimapilis et al. 2018; Raghavendra et al. 2022).

The first mechanism is concerned with the generation of reactive oxygen species (ROS) such as H_2O_2 and induction of cell apoptosis (programmed cell death). The production of ROS put the cell under oxidative stress, causing damage to the cell basic building blocks including DNA, proteins, lipids peroxidation, and eventually cell apoptosis (Siddiqi et al. 2018). This mechanism involves the activation of ZnO-NPs by photocatalytic activity forming electron hole pairs that split the water molecules from the zinc oxide suspension to form $^{\cdot}OH$ and H^+. On the other hand, O_2 molecules tend to yield superoxide anion ($^{\cdot}O^{2-}$) that reacts with H^+ generating $HO_2^{\cdot}$ radicals. The $HO_2^{\cdot}$ radicals interfere with free electrons to generate hydrogen peroxide anion which reacts with H^+ forming hydrogen peroxide molecule (H_2O_2). The produced H_2O_2 penetrates the cell membrane causing sever cell damage and apoptosis. The equations illustrating the above mechanism are available from Padmavathy and Vijayaraghavan (2008). The second proposed mechanism involves the release of Zn^{2+} ions that penetrate to the intracellular contents causing cell damage. This mechanism was supported by a study investigating the toxicity effect of ZnO-NPs against *E. coli* (Li et al. 2008). The third suggested mechanism points to the importance of contact between the nanoparticles and the bacterial cell membrane. According to

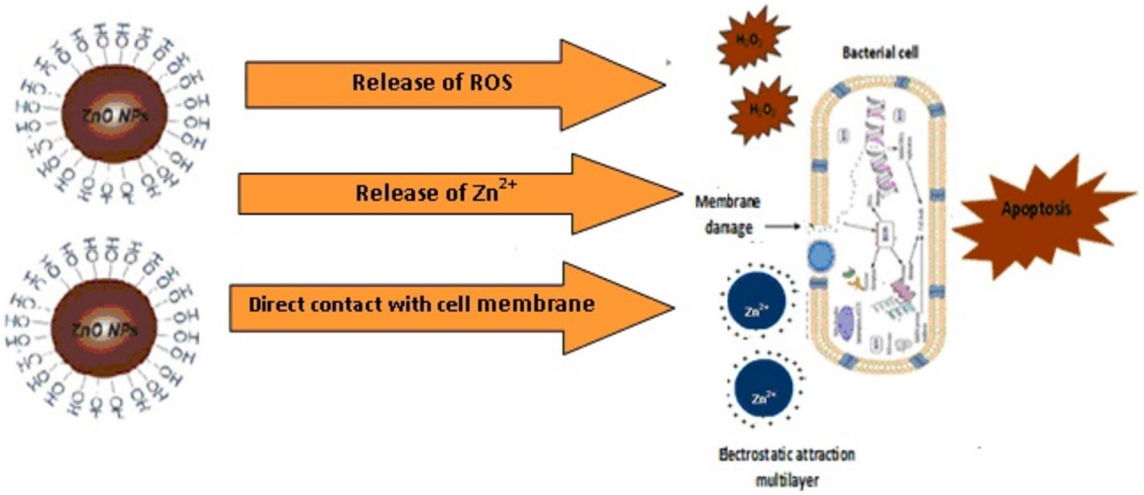

Fig. 8 Disinfection mechanism of phytofabricated ZnO-NPs

Brayner et al. (2006), the direct contact between *E. coli* cell wall and the abrasive ZnO-NPs induced cell wall damage and disorganization, followed by destruction of membrane integrity and a remarkable increase in *E. coli* membrane permeability and finally cells death.

In our case of study, it is worth mentioning that the antibacterial activity was a net result to the synergistic mode of action between the nano-zinc oxide particles as well as the antibacterial activity of *Acacia nilotica* extract. The above suggested mechanism indicates that the phytofabricated ZnO-NPs not only promoted the elimination of *E. coli* cells from aqueous solutions by physical means (adhesion), but also by inhibiting the bacterial growth through efficient bactericidal action.

Conclusions

The current study demonstrates a successful and eco-friendly method for the biosynthesis of ZnO-NPs using green aqueous extract of *Acacia nilotica* pods. These biogenic nanomaterials were examined for their efficiency as novel disinfectants for wastewater and elimination of *E.coli*. The biosynthesized NPs were fully investigated using UV–Vis analysis, XRD, TEM, SEM with EDX, and FTIR characterization. The prepared NPs were hexagonal crystalline structure mainly formed of zincite, whose average size was around 33.87n.m. Several functional groups from the plant extract attributed to flavonoids, phenolics, steroids, terpenoids, and tannins were involved in the process of capping, reducing, and stabilizing of the synthesized NPs. The adhesion capacity studies showed the high potential of ZnO-NPs at 0.5 g disinfectant dose to eliminate *E.coli* from wastewater after 120 min of contact time. Pseudo-second-order kinetics and Freundlich isotherm were best fit describing *E.coli* adhesion mechanism to ZnO-NPs, thus indicating multilayer adhesion over heterogeneous surface and implied that the adhesion was governed by a physical process rather than chemical mechanism. Disinfection mechanism suggested an electrostatic attraction between negatively charged *E.coli* cells and positively charged ZnO-NPs, followed by strong antibacterial activity of ZnO-NPs due to generation of H_2O_2 leading to cell apoptosis. BBD under RSM model suggested a disinfectant dose 30 g/L, contact time 6 h, and *E.coli* concentration 150×10^7 cfu/mL as optimized conditions for 99.8% *E.coli* elimination from wastewater. In attempts for applications, real wastewater samples were treated using the phytofabricated ZnO-NPs immobilized onto sodium alginate beads. The removal efficiencies reached 98.2%, 97.2%, and 96.5% for total coliform, fecal coliform, and *E.coli*, respectively, after 6 h of treatment. ZnO-NPs were sustainable during four consecutive cycles of reuse. In conclusion, phytofabricated ZnO-NPs have the potential to pave the way for efficient and applied wastewater disinfection in an eco-friendly and cost-effective manner. Future perspective of the developed work aims to modify the method of biosynthesis to accomplish ZnO-NPs mass production and recommend implementation for the study outcomes on a large scale for possible wastewater reuse in safe unrestricted irrigation.

Acknowledgements The authors thank and appreciate the microbiology department at the Central Laboratory for Environmental Quality Monitoring, National Water Research Center, Egypt, for the technical and moral support of this work.

Funding Open access funding provided by The Science, Technology & Innovation Funding Authority (STDF) in cooperation with The Egyptian Knowledge Bank (EKB).

Data availability All data generated or analyzed during this study are included in this published article.

Declarations

Conflict of interest The authors declare that they have no competing interests.

Ethical approval Not applicable.

Consent for publication The authors consent to publish the manuscript in "Applied Water Science."

References

Abduljawad EA (2020) Review of some evidenced medicinal activities of *Acacia nilotica*. Arch Pharm Pract 11:20–25

Ahmad I, Beg AZ (2001) Antimicrobial and phytochemical studies on 45 Indian medicinal plants against multidrug resistant human pathogens. J Ethnopharmacol 74:113–123

Akbar N, Aslam Z, Siddiqui R, Shah MR, Khan NA (2021) Zinc oxide nanoparticles conjugated with clinically-approved medicines as potential antibacterial molecules. AMB Express 11:1–6

Al-Samarri GF, Singh H, Syarhabil M (2012) Evaluating eco-friendly botanicals (natural plant extracts) as alternatives to synthetic fungicides. Ann Agric Environ Med 19:673–676

APHA (2017) Standard Methods for the Examination of Water and Wastewater, 23rd edn. American Public Health Association, Washington

Araujo-Lima CF, Nunes RJM, Carpes RM, Aiub FAF, Felzenszwalb I (2017) Pharmacokinetic and toxicological evaluation of a zinc gluconate-based chemical sterilant using in vitro and in silico approaches. Biomed Res Int 2017:5746768

Archana S, Jayanna BK, Ananda A, Ananth MS, Ali AM, Muralidhara HB, Kumar KY (2022) Numerical investigations of response surface methodology for organic dye adsorption onto Mg-Al LDH-GO Nano Hybrid: an optimization, kinetics and isothermal studies. J Indian Chem Soc 99:100249

Arya G, Kumari RM, Pundir R, Chatterjee S, Gupta N, Kumar A, Chandra R, Nimesh S (2019) Versatile biomedical potential of biosynthesized silver nanoparticles from *Acacia nilotica* bark. J Appl Biomed 17(2):115–124

Asadi S, Moeinpour F (2019) Inactivation of Escherichia coli in water by silver-coated $Ni_{0.5}Zn_{0.5}Fe_{0.5}$ magnetic nanocomposite: a Box-Behnken design optimization. Appl Water Sci 9:23

Batanouny KH (1999) Wild medicinal plants in Egypt. An Inventory to support conservation and sustainable Use. Palm Press, Cairo

Bawazeer S, Rauf A, Shash SUA, Shawky AM, Al-Awthan YS, Bahattab OS, Uddin G, Sabir J, El-Esawi MA (2021) Green synthesis of silver nanoparticles using Tropaeolum majus: phytochemical screening and antibacterial studies. Green Process Synthesis 10:85–94

Brayner R, Ferrari-lliou R, Brivois N, Djediat S, Benedetti MF, Fievet F (2006) Toxicological impact studies based on Escherichia coli bacteria in ultrafine ZnO nanoparticles colloidal medium. Nano Lett 6:866–870

Dimapilis EAS, Hsu C, Mendoza RMO (2018) Zinc oxide nanoparticles for water disinfection. Sustain Environ Res 28:47–56

Elumalai K, Velmurugan S (2015) Green synthesis, characterization and antimicrobial activities of zinc oxide nanoparticles from the leaf extract of *Azadirachta indica* (L.). Appl Surf Sci 345:329–336

Espitia PJP, Soares NFF, Coimbra JSR, Andrade NJ, Cruz RS, Medeiros EAA (2015) Zinc oxide nanoparticles: synthesis, antimicrobial activity and food packaging applications. Food Bioprocess Technol 5:1447–1464

Ettadili FE, Aghris S, Laghrib F, Farahi A, Saqrane S, Bakasse M, Lahrich S (2022) Recent advances in the nanoparticles synthesis using plant extract: applications and future recommendations. J Mol Struct 1248:131538

Foo KY, Hameed BH (2010) Insights into the modeling of adsorption isotherm systems. Chem Eng J 156:2–10

Gupta M, Tomar RS, Kaushik S, Mishra RK, Sharma D (2018) Effective antimicrobial activity of green ZnO nano particles of *Catharanthus roseus*. Front Microbiol 9:2030

Gurgur E, Oluyamo SS, Adetuyi AO, Omotunde OI, Okoronkwo AE (2020) Green synthesis of zinc oxide nanoparticles and zinc oxide–silver, zinc oxide–copper nanocomposites using *Bridelia ferruginea* as biotemplate. SN Appl Sci 2:1–12

Hameed FR, Mukalaf AA, Kareem AA, Yousif WT, Dhumad BQ (2017) Antimicrobial effect of *Acacia nilotica* on some Gram positive and Gram negative bacteria. Al-Mustansiriyah Journal of Science 28:14–19

Happy A, Soumya M, Kumar SV, Rajeshkumar S, Sheba RD, Lakshmi T, Nallaswamy VD (2019) Phyto-assisted synthesis of zinc oxide nanoparticles using *Cassia alata* and its antibacterial activity against *Escherichia coli*. Biochem Biophys Rep 17:208–211

Harborne JB (1998) Phytochemical Methods. Chapman and Hall Publications, London, pp 7–8

Heidrum S, Hans A (2006) High pressure X-ray investigation of zincite ZnO single crystal using diamond anvils with an improved shape. J Appl Crystallogr 39:169–175

Hemlata MPR, Singh AP, Tejavath KK (2020) Biosynthesis of silver nanoparticles using *Cucumis prophetarum* aqueous leaf extract and their antibacterial and antiproliferative activity against cancer cell lines. ACS Omega 5:5520–5528

Hessien M, Taha A, Da'na E (2022) *Acacia nilotica* Pods' extract assisted-hydrothermal synthesis and characterization of ZnO-CuO nanocomposites. Materials 15:2291

Hooshyari G (2017) Ealuating Filter Materials for *E. coli* Removal from Storm water. Theses and Dissertations. 126

Iravani S (2011) Green synthesis of metal nanoparticles using plants. Green Chem 13:2638–2650

Jadhav SB, Surwase SN, Phugare SS, Jadhav JP (2013) Response surface methodology mediated optimization of remazol orange decolorization in plain distilled water by *Pseudomonas aeruginosa* BCH. Int J Environ Sci Technol 10:181–190

Jafari AJ, Kakavandi B, Kalantary RR, Gharibi H, Asadi A, Azari A, Babaei AA, Takdastan A (2016) Application of mesoporous magnetic carbon composite for reactive dyes removal: Process optimization using response surface methodology. Korean J Chem Eng 33:2878–2890

Jame R (2018) Phytochemical and pharmacological uses of Acacia nilotica- a review. Int J Bioorg Chem 3:6–10

Kaur P, Arora S, Singh R (2022) Isolation, characterization and biological activities of betulin from *Acacia nilotica* bark. Sci Rep 12:9370

Li Q, Mahendra S, Lyon DY, Brunet L, Liga MV, Li D, Alvarez PJJ (2008) Antimicrobial nanomaterials for water disinfection and microbial control: potential applications and implications. Water Res 42:4591–4602

Lopes de Romana DL, Brown KH, Guinard JX (2002) Sensory trial to assess the acceptability of zinc fortificants added to iron-fortified wheat products. J Food Sci 67:461–465

Ma C, Ihara M, Liu S, Sugie Y, Tanaka H (2022) Tracking the source of antibiotic-resistant *Escherichia coli* in the aquatic environment in Shiga, Japan, through whole-genome sequencing. Environmental Advances 8:100185

Mahendra C, Murali M, Manasa G, Ponnamma P, Abhilash MR, Lakshmeesha TR, Satish A, Amruthesh KN, Sudarshana MS (2017) Antibacterial and antimitotic potential of bio-fabricated zinc oxide nanoparticles of *Cochlospermum religiosum* (L.). Microb Pathog 110:620–629

Mallakpour S, Sirous F, Hussain CMA (2021) Journey to the world of fascinating ZnO nanocomposites made of chitosan, starch, cellulose, and other biopolymers: Progress in recent achievements in eco-friendly food packaging, biomedical, and water remediation technologies. Int J Biol Macromol 170:701–716

Mostafaii G, Chimehi E, Gilasi H, Iranshahi L (2017) Investigation of zinc oxide nanoparticles effects on removal of total coliform bacteria in activated sludge process effluent of municipal wastewater. J Environ Sci Technol 10:49–55

Mydeen SS, Kumar RR, Kottaisamy M, Vasantha VS (2020) Biosynthesis of ZnO nanoparticles through extract from *Prosopis juliflora* plant leaf: antibacterial activities and a new approach by rust-induced photocatalysis. J Saudi Chem Soc 24:393–406

Natrah S, Bakil A, Kamal H, Abdullah HZ, Idris MI (2020) Sodium alginate-zinc oxide nanocomposite film for antibacterial wound healing applications. Biointerface Res Appl Chem 10:6245–6252

Nikiel CA, Eltahir EAB (2021) Past and future trends of Egypt's water consumption and its sources. Nat Commun 12:4508

Nkhabinze BZ, Wanyika HN, Earnshaw DM, Elijah MA (2022) Synthesis of silver nanoparticles using crude leaf extracts of *Acacia nilotica*, *Azadirachta indica*, *Carissa spinarum*, *Melia azedarach*, *Senna didymobotrya* and *Warburgia ugandensis*, and their antifungal activity against *Sporisorium scitamineum*. Afr J Biotech 21:305–313

Pachaiappan R, Rajendran S, Ramalingam G, Vo DN, Priya PM, Soto-Moscoso M (2021) Green synthesis of zinc oxide nanoparticles by *Justicia adhatoda* leaves and their antimicrobial activity. Chem Eng Technol 44:551–558

Padmavathy N, Vijayaraghavan R (2008) Enhanced bioactivity of ZnO nanoparticles-an antimicrobial study. Sci Technol Adv Mater 9:035004

Perez CM, Pauli M, Bazerque P (1990) An antibiotic assay by agar well diffusion method. Acta Biologiae Et Medicinae Experimentalis 15:113–115

Primo J, Horsth DF, Correa J, Das A, Bittencourt C, Umek P, Buzanich AG, Radtke M, Yusenko KV, Zanette C, Anaissi FJ (2022) Synthesis and characterization of Ag/ZnO nanoparticles for bacteria disinfection in water. Nanomaterials 12:1764

Raghavendra VB, Shankar S, Govindappa M, Pugazhendhi A, Sharma M, Nayaka SC (2022) Green synthesis of zinc oxide nanoparticles (ZnO NPs) for effective degradation of dye, polyethylene and antibacterial performance in wastewater treatment. J Inorg Organomet Polym Mater 32:614–630

Rasha E, Monerah A, Manal A, Rehab A, Mohammed D, Doaa E (2021) Biosynthesis of zinc oxide nanoparticles from *Acacia nilotica* (L.) extract to overcome carbapenem-resistant Klebsiella pneumoniae. Molecules 26:1919

Rasheed PA, Jabbar KA, Rasool K, Pandey RP, Sliem MH, Helal M, Samara A, Abdullah AM, Mahmoud KA (2019) Controlling the biocorrosion of sulfate-reducing bacteria (SRB) on carbon steel using ZnO/chitosan nanocomposite as an eco-friendly biocide. Corros Sci 148:397–406

Salam A, Khan AR, Liu L, Yang S, Azhar W, Ulhassan Z, Zeeshan M, Wu J, Fan X, Gan Y (2022) Seed priming with zinc oxide nanoparticles downplayed ultrastructural damage and improved photosynthetic apparatus in maize under cobalt stress. J Hazard Mater 423:127021

Saratale RG, Saratale GD, Cho SK, Ghodake G, Kadam A, Kumar S, Mulla SI, Kim DS, Jeon B, Chang JS, Chang JS, Shin HS (2019) Phyto-fabrication of silver nanoparticles by *Acacia nilotica* leaves: Investigating their antineoplastic, free radical scavenging potential and application in H_2O_2 sensing. J Taiwan Inst Chem Eng 99:239–249

Sheny DS, Mathew J, Pilip D (2011) Phytosynthesis of Au, Ag and Au-Ag bimetallic nanoparticles using aqueous extract and dried leaf of Anacardium occidentale. Spectrochim Acta Part A Mol Biomol Spectrosc 79:254–262

Siddiqi KS, Rahman AU, Husen A, Husen T (2018) Properties of zinc oxide nanoparticles and their activity against microbes. Nanoscale Res Lett 13:141

Singh K, Singh J, Rawat M (2019) Green synthesis of zinc oxide nanoparticles using *Punica Granatum* leaf extract and its application towards photocatalytic degradation of Coomassie brilliant blue R-250 dye. SN Appl Sci 1:1–8

Singh H, Kumar A, Thakur A, Kumar P, Nguyen VH, Vo DV, Sharma A, Kumar D (2020) One-pot synthesis of magnetite-ZnO nanocomposite and its photocatalytic activity. Top Catal 63:1097–1108

Sohail MF, Rehman M, Hussain SZ, Huma ZE, Shahnaz G, Qureshi OS, Webster TJ (2020) Green synthesis of zinc oxide nanoparticles by Neem extract as multi-facet therapeutic agents. J Drug Deliv Sci Technol 59:101911

Souza VG, Rodrigues C, Valente S, Pimenta C, Pires JR, Alves MM, Santos CF, Coelhoso IM, Fernando AL (2020) Eco-friendly ZnO/Chitosan bionanocomposites films for packaging of fresh poultry meat. Coatings 10:110

Spoiala A, Ilie C-I, Trusca R-D, Oprea O-C, Surdu V-A, Vasile BS, Ficai A, Ficai D, Andronescu E, Ditu L-M (2021) Zinc oxide nanoparticles for water purification. Materials 14:4747

Sundrarajan M, Ambika S, Bharathi K (2015) Plant-extract mediated synthesis of ZnO nanoparticles using *Pongamia pinnata* and their activity against pathogenic bacteria. Adv Powder Technol 26:1294–1299

Umamaheswari A, Prabu SL, John SA, Puratchikody A (2021) Green synthesis of zinc oxide nanoparticles using leaf extracts of Raphanus sativus var. Longipinnatus and evaluation of their anticancer property in A549 cell lines. Biotechnol Rep 29:e00595

Verma A, Mehata MS (2016) Controllable synthesis of silver nanoparticles using Neem leaves and antimicrobial activity. J Radiat Res Appl Sci 9:109–115

Vijayakumar S, Vaseeharan B, Malaikozhundan B, Shobiya M (2016) *Laurus nobilis* leaf extract mediated green synthesis of ZnO nanoparticles: Characterization and biomedical applications. Biomed Pharmacother 84:1213–1222

Vijayakumar S, Krishnakumar C, Arulmozhi P, Mahadevan S, Parameswari N (2018) Biosynthesis, characterization and antimicrobial activities of zinc oxide nanoparticles from leaf extract of Glycosmis pentaphylla (Retz.) DC. Microb Pathog 116:44–48

Wang L, Hu C, Shao L (2017) The antimicrobial activity of nanoparticles: present situation and prospects for the future. Int J Nanomed 12:1227–1249

Wang L, Wu W, Xie X, Chen H, Lin J, Dionysiou D (2018) Removing *Escherichia coli* from water using zinc oxide-coated zeolite. Water Res 141:145–151

Wang L, Dionysiou DD, Wu W, Chen H, Xie X, Lin J (2019) Zinc oxide-coated zeolite adsorbs and inactivates waterborne *Staphylococcus aureus*. Chemosphere 229:1–7

WHO (2006) Guidelines for the Safe Use of Wastewater, Excreta and Greywater. World Health Organization, Geneva

Yadav M, Singh NK (2017) Isotherm investigation for the sorption of fluoride onto bio-F: comparison of linear and non-linear regression method. Appl Water Sci 7:4793–4800

Zhang L, Jiang Y, Ding Y, Povey M, York D (2007) Investigation into the antibacterial behaviour of suspensions of ZnO nanoparticles (ZnO nanofluids). J Nanopart Res 9:479–489

Zhang DD, Zhao JF, Tan LQ, Wu Q, Lv HX, Zhang YR, Zhang M (2024) Effects of zinc oxide nanocomposites on microorganism growth and protection of physicochemical quality during maize storage. Int J Food Microbiol 411:110552

Zhou XQ, Hayat Z, Zhang DD, Li MY, Hu S, Wu Q, Cao YF, Yuan Y (2023) Zinc Oxide nanoparticles: synthesis, characterization, modification, and applications in food and agriculture. Processes 11:1193